Geomorphology 370 (2020) 107396

Contents lists available at ScienceDirect

Geomorphology

journal homepage: www.elsevier.com/locate/geomorph

New insights into the formation of submarine glacial landforms from high-resolution Autonomous Underwater Vehicle data

Christine L. Batchelor [a,b,*], Aleksandr Montelli [b], Dag Ottesen [c], Jeffrey Evans [d], Evelyn K. Dowdeswell [b], Frazer D.W. Christie [b], Julian A. Dowdeswell [b]

[a] Norwegian University of Science and Technology (NTNU), N-7491 Trondheim, Norway
[b] Scott Polar Research Institute, University of Cambridge, Cambridge CB2 1ER, UK
[c] Geological Survey of Norway (NGU), Postboks 6315, Sluppen, Trondheim N-7491, Norway
[d] Geography and Environment, Loughborough University, Epinal Way, Loughborough, Leicestershire LE11 3TU, UK

ARTICLE INFO

Article history:
Received 3 June 2020
Received in revised form 11 August 2020
Accepted 21 August 2020
Available online 27 August 2020

Keywords:
Autonomous Underwater Vehicles
Glacial landforms
Grounding-zone wedge
Iceberg ploughmarks
Corrugation ridges
Antarctic Peninsula

ABSTRACT

Autonomous Underwater Vehicles (AUVs) deployed close to the seafloor can acquire high-resolution geophysical data about the topography and shallow stratigraphy of the seabed, yet have had limited application within the fields of glacial geomorphology and ice sheet reconstruction. Here, we present multibeam echo-sounding, side-scan sonar, sub-bottom profiler and High-Resolution Synthetic Aperture Sonar (HISAS) data acquired during three AUV dives on the northeast Antarctic Peninsula continental shelf. These data enable glacial landforms, including mega-scale glacial lineations (MSGLs), grounding-zone wedges (GZWs) and iceberg ploughmarks, to be imaged at a horizontal resolution of a few tens of centimetres, allowing for the identification of subtle morphological features. We map tidal ridges that are interpreted as having been formed 1) along the ice-sheet grounding line by the squeezing up of soft seafloor sediments by vertical motion of the grounding line during tidal cycles, and 2) by the tidally driven motion of grounded or near-grounded icebergs. These data also enable the mapping of small GZWs that show the location of short-term still-stands or re-advances of the ice-sheet grounding zone. No meltwater channels are identified from our data, suggesting that free-flowing meltwater may not be essential for the formation of GZWs or MSGLs. The examples presented here show how high-resolution AUV-derived geophysical data provide a step-change in our ability to image seafloor glacial landforms, enabling new interpretations about past ice dynamics and glacial sedimentation at fine temporal and spatial scales.

1. Introduction

The analysis of glacial landforms preserved on and beneath the seafloor of formerly glaciated continental margins provides information about the past dynamic behaviour of glaciers and ice sheets (e.g. Dowdeswell et al., 2008a, 2016; Greenwood et al., 2012) and the mechanisms by which sediment is eroded, transported and deposited by ice (e.g. Lowe and Anderson, 2003; Dowdeswell et al., 2004; Spagnolo et al., 2014). Submarine glacial landforms are typically mapped using geophysical data acquired from hull-mounted sonar systems. Recent seafloor mapping programmes and subsurface investigations, including offshore of Greenland (OMG Mission, 2016), Arctic Canada (www.omg.unb.ca/arctic-mapping/) and Norway (www.mareano.no), have greatly increased data coverage of formerly ice-covered fjords and continental shelves. Typical assemblages of glacial landforms, for example those indicating the former presence of fast-flowing ice streams (e.g. Stokes and Clark, 1999; Ó Cofaigh et al., 2002; Dowdeswell et al., 2014) and surging glaciers (e.g. Evans and Rea, 1999; Ottesen et al., 2008; Dowdeswell and Ottesen, 2016), have become well-established, facilitating ice-sheet-wide interpretations of the past configuration and dynamics of ice sheets (e.g. Anderson et al., 2002; Ottesen et al., 2005; Ó Cofaigh et al., 2014; Batchelor et al., 2019a).

The acquisition of high-resolution geophysical data is necessary to examine complexities in ice-sheet behaviour recorded in seafloor geomorphology. Individual sectors of former ice sheets have been shown to have experienced complex and variable responses to past climatic changes (Greenwood et al., 2012; Smedley et al., 2017). In addition, there is no consensus on the formation mechanisms of some glacial landforms, particularly subglacial bedforms such as mega-scale glacial lineations (MSGLs) (Clark et al., 2003; Stokes et al., 2011; Fowler and Chapwanya, 2014). High-frequency sonar systems provide information about the seafloor and subsurface at a higher spatial resolution compared with lower-frequency sonar, albeit with a shorter water-depth range. The use of sonar equipment mounted on Autonomous Underwater Vehicles (AUVs) enables a high-frequency acoustic signal to be transmitted through the water at a few tens of metres from the

* Corresponding author at: Norwegian University of Science and Technology (NTNU), N-7491 Trondheim, Norway.
E-mail address: clb70@cam.ac.uk (C.L. Batchelor).

https://doi.org/10.1016/j.geomorph.2020.107396

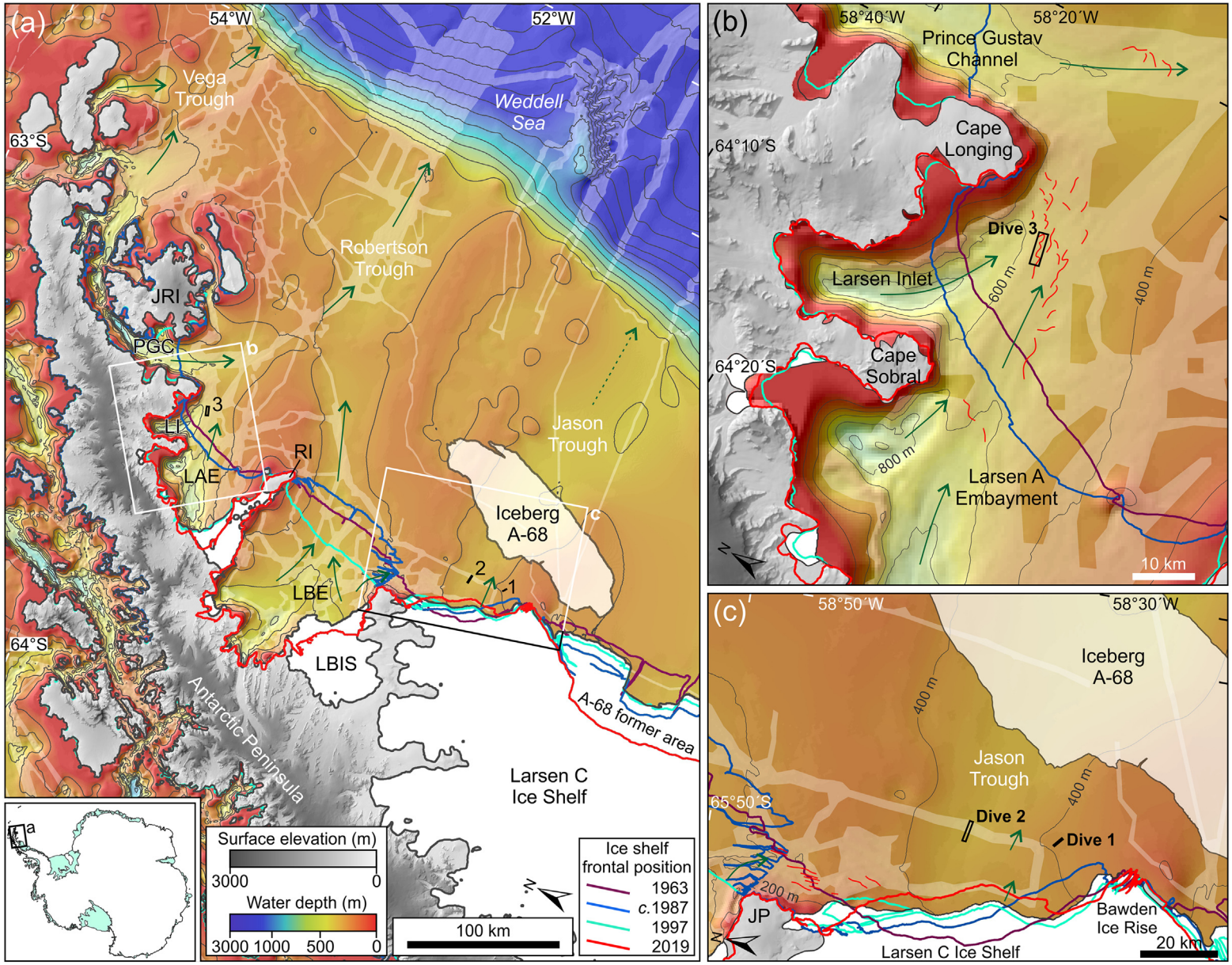

Fig. 1. Location of the three Autonomous Underwater Vehicle (AUV) surveys (dives 1–3). (a) Map showing the bathymetry around the NE Antarctic Peninsula. Green arrows indicate former ice-flow direction implied by previously reported streamlined submarine landforms (Evans et al., 2005; Lavoie et al., 2015; Evans and Hogan, 2016; Campo et al., 2017); dashed, probable former ice-flow direction through Jason Trough. The *c.*1987 and 1997 ice shelf frontal positions are from Cook and Vaughan (2010), and the 1963 ice shelf frontal position was digitised from declassified Argon satellite imagery (Kim et al., 2007). The 2019 ice front was derived using ESA/Copernicus Sentinel-1a/b imagery acquired in January 2019. The position of iceberg A-68 on 12 January 2019 is also shown. The Antarctic coast and grounding line (dark grey) is from Depoorter et al. (2013). Bathymetry is from the International Bathymetric Chart of the Southern Ocean (IBCSO; Arndt et al., 2013), with 200 m contours. Translucent shading shows existing bathymetric data coverage. Surface elevation is from the Reference Elevation Model of Antarctica (REMA; Howat et al., 2019). JRI = James Ross Island; LAE = Larsen A Embayment; LBE = Larsen B Embayment; LBIS = Larsen B Ice Shelf; LI = Larsen Inlet; PGC = Prince Gustav Channel; RI = Robertson Island. Inset shows the location of the study area in Antarctica. (b) Detail of the location of AUV dive 3. Thin red lines are former grounding zone positions interpreted from hull-mounted multibeam echo-sounder data (Evans et al., 2005; Lavoie et al., 2015; Evans and Hogan, 2016; Campo et al., 2017). (c) Detail of the location of AUV dives 1 and 2. JP = Jason Peninsula.

seafloor. Geophysical data collected from AUVs can, therefore, be of significantly higher horizonal resolution (often <1 m) compared with data collected from conventional, hull-mounted sonar systems (typically several metres or tens of metres), although AUV data are typically acquired over narrower swaths of the seafloor. Although AUVs have been used extensively by the hydrocarbon industry and in marine archaeological studies (Bingham et al., 2010; Bates et al., 2011; Ødegård et al., 2018), they have hitherto had limited application within the field of glacial geomorphology (Dowdeswell et al., 2008b, 2020a; Graham et al., 2013; Howe et al., 2019).

In this paper, we present high-resolution geophysical data collected from AUVs in three locations on the northeast (NE) Antarctic Peninsula continental shelf (Fig. 1) as examples of the fine detail that can be achieved using multibeam-equipped AUVs operating close to the seafloor. We map the distribution of subglacial, ice-marginal and proglacial landforms, and provide new interpretations for the subdued forms that are identified from these data. Geophysical data acquired from AUVs are discussed in terms of their implications for revealing complexities in past ice-sheet behaviour and understanding processes and patterns of glacier-influenced sedimentation.

2. Regional geological and glaciological setting

Geophysical data show that there is a seaward transition from exposed or near-surface bedrock on the inner shelf of the NE Antarctic Peninsula to a mid- to outer shelf sedimentary substrate (Bentley and Anderson, 1998; Anderson et al., 2002; Gilbert et al., 2003; Evans et al., 2005). The continental shelf is incised by a number of cross-shelf troughs that were occupied and eroded by fast-flowing ice streams of the Antarctic Peninsula Ice Sheet (APIS) during successive full-glacial periods (The RAISED Consortium, 2014). Three major cross-shelf troughs, which are more than 1000 m deep in their inner parts and 400–600 m deep on the mid- to outer shelf, are present between 63°S and 67°S along the NE Antarctic Peninsula (Fig. 1): Vega Trough, which is north of James Ross Island; Robertson Trough, which is connected to deep tributary troughs in Prince Gustav Channel, Larsen Inlet, and the Larsen A and Larsen B embayments via a broad mid-shelf trough south and southeast of James Ross Island (Domack et al., 2001; Evans et al., 2005); and Jason Trough, which extends from Larsen C Ice Shelf to the shelf break (Fig. 1). The troughs are separated by shallower banks that are between 200 and 400 m deep.

North of about 66°S, ship-based operations have acquired significant geophysical and geological data about the seafloor and subsurface, particularly from the inner shelf (Sloan et al., 1995; Anderson, 1999; Domack et al., 2001; Pudsey and Evans, 2001; Pudsey et al., 2001; Camerlenghi et al., 2002; Evans and Pudsey, 2002; Brachfeld et al., 2003; Gilbert et al., 2003; Evans et al., 2005; Heroy and Anderson, 2005; Arndt et al., 2013). The distribution of glacial landforms preserved on the seafloor has informed reconstructions of the configuration and dynamics of the eastern APIS as it retreated from the shelf break during the last deglaciation (Evans et al., 2005; Reinardy et al., 2011; Ó Cofaigh et al., 2014; The RAISED Consortium, 2014; Lavoie et al., 2015; Campo et al., 2017). Relative palaeomagnetic intensity dating of sediment cores suggests that the transition from grounded ice to ice shelf in the Larsen A and Larsen B embayments occurred before *c.* 10.7 cal. ka BP (Brachfeld et al., 2003; Evans et al., 2005; Domack et al., 2005; Ó Cofaigh et al., 2014).

Comparatively little is known about the seafloor and substrate south of about 66°S (Fig. 1a) because of the sea ice that typically persists in this area even during the austral summer (Kurtz and Markus, 2012; Dowdeswell et al., 2020b). The limited bathymetric data that are available offshore of Larsen C Ice Shelf (Fig. 1c) show that the shallow banks on either side of Jason Trough are heavily scoured by iceberg ploughmarks (Dowdeswell et al., 2020b). The APIS probably reached the shelf break beyond Larsen C Ice Shelf during the LGM, about 20 ka, and was likely close to its present-day configuration by about 10 ka (Ó Cofaigh et al., 2014; The RAISED Consortium, 2014).

Since satellite imagery first became available in the 1960s, an overall reduction in the area of the floating ice shelves along the NE Antarctic Peninsula has been observed (Fig. 1). Major ice-shelf collapses occurred in Larsen Inlet in 1989, Larsen A Embayment and Prince Gustav Channel in 1995, and Larsen B Embayment in 2002 (Doake and Vaughan, 1991; King, 1994; Vaughan and Doake, 1996; Rott et al., 1996; Skvarca et al., 1999; Scambos et al., 2003; Rack and Rott, 2004; Cook and Vaughan, 2010). These collapse events have been linked to increases in regional surface air temperatures (Fahnestock et al., 2002; Morris and Vaughan, 2003; Vaughan et al., 2003; Scambos et al., 2003) and ocean-driven basal melting over the past few decades (Shepherd et al., 2004; Adusumilli et al., 2018). Upstream, the now unrestrained tributary glaciers that once nourished these ice shelves have retreated, greatly accelerating the Antarctic Peninsula's total contribution to global sea-level rise (Rott et al., 2002, 2011, 2018; De Angelis and Skvarca, 2003; Rignot et al., 2004; Scambos et al., 2004; Pritchard et al., 2009; Shepherd et al., 2018). The dynamic disintegration of the ice shelves on the NE Antarctic Peninsula thus provides motivation to understand the past dynamic behaviour of the ice sheet and ice shelves in this region.

3. Methods

3.1. Geophysical data acquired from Autonomous Underwater Vehicles (AUVs)

Geophysical data were acquired from the NE Antarctic Peninsula continental shelf using two Kongsberg HUGIN 6000 AUVs, which were deployed from the SA *Agulhas II* in January 2019. AUV 7 operated in downwards-looking mode only and was equipped with a multibeam echo-sounder, sub-bottom profiler and side-scan sonar (Fig. 2) (cf. Jakobsson et al., 2016). AUV 9 was constructed to operate in upward- or downward-looking mode and was equipped with a downward-looking sub-bottom profiler and High-Resolution Synthetic Aperture Sonar (HISAS), as well as an upward-looking multibeam echo-sounder. Details of the geophysical survey equipment used in this study are shown in Table 1.

The multibeam echo-sounder on AUV 7 was operated at a frequency of 400 kHz, with 400 beams and a maximum port- and starboard-side beam angle of 60°. Initial processing of the multibeam echo-sounder and navigation data was performed using EIVA and Navlab software. The data were adjusted for tidal variations relative to the WGS84 Ellipsoid, and a low-pass filter was applied to remove erroneous depth soundings. The bathymetric data acquired 60 or 70 m above the seafloor have a horizontal resolution of ~0.5 m and were gridded at a cell-size of 1 m, whereas the data acquired at a height of 10 m have a horizontal resolution of ~0.1 m and were gridded at a cell-size of 0.2 m. Fledermaus software was used to grid and visualise these data.

The AUV-mounted sub-bottom profilers were operated with a pulse bandwidth of 1–11 kHz and a pulse length of 20 ms. The horizontal and vertical resolution of these data are ~0.5 m and 0.1 m, respectively. In the study area, the penetration depth of the sub-bottom profiler was restricted to ~5–15 m in acoustically transparent to layered sediments, as a result of the relatively coarse and often diamictic subsurface sediments on glacier-influenced continental shelves (e.g. Dowdeswell et al., 2004).

Side-scan sonar imagery can be acquired with a greater total swath width compared with multibeam echo-sounders, although with a data gap along the line of acquisition (Fig. 2). For example, in this study, a total swath width of ~1300 m was produced when the AUV was flown at a height of 70 m above the seafloor compared with ~200 m for the multibeam swath width, but with a gap of ~60 m beneath the vehicle. The side-scan sonar on AUV 7 was operated at 75 kHz (Table 1).

In addition to acquiring high-resolution images of the seafloor, the interferometric capability of HISAS systems enables the depth of the seafloor to be estimated directly (Lurton, 2010; Sæbø et al., 2013; Ødegård et al., 2018). The HISAS on AUV 9 has a frequency range of 60–120 kHz (Table 1). It was used to acquire images of the seafloor with a horizontal

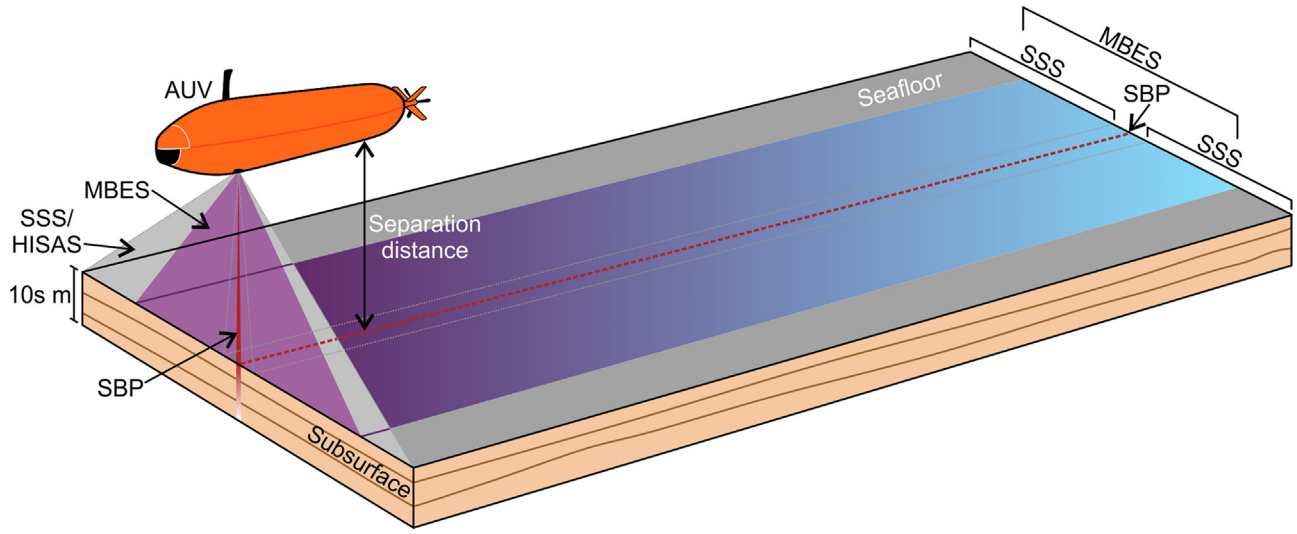

Fig. 2. Schematic showing the different types of geophysical data that were acquired using AUVs in this study. HISAS = High-Resolution Synthetic Aperture Sonar; MBES = multibeam echo-sounding; SBP = sub-bottom profiling; SSS = side-scan sonar.

resolution of ~0.05 m, which were processed to produce bathymetry with a horizontal resolution of ~0.5 m. Processing of the sub-bottom profiler, side-scan sonar and HISAS data was performed onboard SA *Agulhas II* using Delph software.

Geophysical data about the seafloor and shallow subsurface of the NE Antarctic Peninsula continental shelf were acquired during three AUV dives (Fig. 1 and Table 2). The speed of the AUVs during data collection was between 3.2 and 3.6 knots. The AUVs were used in bottom-tracking mode, which maintained a fixed separation distance between the vehicle and the seafloor. A variety of seafloor separation distances, ranging from 10 to 70 m (Table 2), was used to compare the resolution of the AUV-derived data at different heights above the seafloor.

3.2. Geophysical data acquired from hull-mounted sonar

For comparative purposes with our AUV-derived seafloor imagery, we also show bathymetric data from the well-surveyed mid-Norwegian margin that were collected as part of the Mareano programme (www.mareano.no). These data provide analogues for some of the seafloor features identified from the NE Antarctic Peninsula continental shelf. The Mareano data illustrated in this paper were collected in 2011 and 2014 using a hull-mounted multibeam echo-sounder that operated at frequencies in the 70–100 kHz range (Table 1). When deployed in water depths of less than around 500 m, the relatively high-frequency of this sonar enabled the collection of bathymetric data with a horizonal resolution of a few metres.

4. Results

We present high-resolution AUV-acquired geophysical data of landforms from formerly subglacial, ice-marginal and proglacial environments on the NE Atlantic Peninsula continental shelf (Fig. 1).

4.1. Mega-scale glacial lineations (MSGLs) – subglacial

Parallel to sub-parallel elongate ridges up to 50 m wide, several metres high and 0.1–3 km long, with elongation ratios of up to 60:1, are identified along the central axis of Jason Trough (dive 2; Fig. 1c) on HISAS-derived bathymetry (Fig. 3a–d). These ridges are interpreted as MSGLs (e.g. Stokes and Clark, 2002; Dowdeswell et al., 2004; King et al., 2009; Spagnolo et al., 2014) that were formed beneath an ice stream that extended through Jason Trough during the last glacial cycle. Although MSGLs have been mapped previously at the southern lateral margin of Jason Trough (Fig. 1c) (Lavoie et al., 2015; Campo et al., 2017), this is the first time that they have been identified in the central, deepest axis of the trough. The MSGLs overprint sedimentary wedges that are up to 5 m high (Fig. 3a and b), which are interpreted as small grounding-zone wedges (GZWs) (see Section 4.2). The subtle changes in orientation of the MSGLs across the GZW surfaces (Fig. 3a and b) probably reflect small-scale adjustments in local ice-flow direction during deglaciation.

The MSGLs are also visible on sub-bottom profiles (Fig. 3e). Three acoustic facies, corresponding to three acoustic units, are identified from sub-bottom profiles in Jason Trough (Fig. 3e and f). The uppermost unit is acoustically semi-transparent, up to 5 m thick and has a draping geometry (Fig. 3e and f). The unit beneath is faintly acoustically stratified, around 3 m thick and also has a draping appearance. These two uppermost units are interpreted as glacimarine sediment (Stoker, 1988; Ó Cofaigh and Dowdeswell, 2001), a proportion of which may have been deposited beneath a floating ice shelf (e.g. Evans and Pudsey, 2002). The MSGLs that are expressed on the seafloor inherit their geometry from the irregular surface of the third, lowermost, acoustic unit in Jason Trough (Fig. 3e and f). The acoustically transparent character of this unit, together with its association with MSGLs and position beneath a stratified unit interpreted as glacimarine sediment, suggests that it is

Table 1
Acquisition details for the geophysical data shown in this paper. HISAS = High-Resolution Synthetic Aperture Sonar; MBES = multibeam echo-sounder; SBP = sub-bottom profiler; SSS = side-scan sonar.

Cruise details	Data	System	Frequency (kHz)
AUVs launched from SA *Agulhas II*; 2019	MBES	Kongsberg EM2040	200–400
	SBP	EdgeTech Chirp	2–16
	SSS	EdgeTech 2205	75, 230 or 400
	HISAS	HISAS 1030	60–120
Survey vessel *Franklin*; Mareano programme; 2011	MBES	Kongsberg EM710	70–100
Fosae survey vessels; Mareano programme; 2014	MBES	Kongsberg EM710	70–100

Table 2
Details of the data collected during three survey dives of the AUVs launched from the SA *Agulhas II* in 2019.

Dive	AUV	Equipment	Separation (m)	Survey size
1: Southern lateral margin of Jason Trough	7	MBES	60	0.6 km^2
		MBES	10	0.075 km^2
		SBP	60	4.1 line-km
		SSS	60	6.1 km^2
2: Central Jason Trough	9	SBP	25	13 line-km
		HISAS	25	4 km^2
3: Larsen Inlet	7	MBES	70	8.6 km^2
		SBP	70	64 line-km
		SSS	70	40 km^2

subglacial traction till (Licht et al., 1999; Dowdeswell et al., 2004; Livingstone et al., 2016). At up to 3 m thick, this unit is of a similar thickness to a layer of 'soft' subglacial traction till in which MSGLs are formed in Marguerite Trough on the western Antarctic Peninsula, which has an average thickness of 4.6 m (Dowdeswell et al., 2004; Evans et al., 2005; Ó Cofaigh et al., 2005, 2007). The base of the lowermost acoustic unit in Jason Trough is marked by a high-amplitude, relatively flat-lying impenetrable reflection (Fig. 3e and f). This reflection is interpreted as the surface of a firmer subglacial traction till, which may be similar to the 'stiff till' that was reported from Marguerite Trough (Dowdeswell et al., 2004; Ó Cofaigh et al., 2005).

HISAS images reveal the seafloor expression of the MSGLs at unprecedented resolution, showing that the seaward and landward ends of these features are not associated with any obstacles or recognisable change in substrate (Fig. 3g). Narrow (1–2 m wide) linear forms are identified along the crests of some of the elongate ridges ('striations' in Fig. 3g), which are interpreted to have been formed by the fine-scale streamlining of the deformable sediment that comprises the MSGLs in the direction of ice flow.

Individual clasts up to 1 m high are imaged on or close to the seafloor on HISAS images (Fig. 3g). We do not discern any pattern in the distribution of these clasts across the surveyed area. The clasts are interpreted as ice-rafted debris (IRD) that was released either from the base of Larsen C Ice Shelf when it was at an advanced position beyond its modern frontal limits, or from freely drifting icebergs. The 'fresh' appearance of the clasts suggests that the icebergs that calve from the modern Larsen C Ice Shelf (Fig. 1c) transfer significant quantities of relatively large IRD clasts to the surveyed area where they are released from the icebergs by melting and/or overturning. The high concentration of IRD on the seafloor of Jason Trough (Figs. 3g and 4e) may be linked to the proximity of this site to the mountainous Jason Peninsula (Fig. 1c), which provides an area from which the debris could be sourced.

4.2. Grounding-zone wedges (GZWs) – ice-marginal

In Jason Trough (dive 2; Fig. 1c), a series of four sedimentary wedges is identified on HISAS-derived bathymetry at approximately 500 m water depth (Figs. 3a and 4a). The four wedges partially overlie each other, with the youngest wedge present only towards the north of the surveyed area (Fig. 3b). The sides of the wedges are up to 5 m high (Fig. 4c) and have a smooth expression on HISAS images (Fig. 4e). The wedges are associated with a transparent to chaotic acoustic unit, interpreted as 'soft' subglacial traction till, which pinches out where the wedges are not present (Fig. 3f). The roughly ice-flow-parallel orientation of the wedges (Fig. 4a) suggests that the AUV surveyed the lateral margins of a complex of stacked GZWs. GZWs record the former positions of still-stands or re-advances in the ice-sheet grounding zone and are usually oriented transverse-to-flow (e.g. King et al., 1991; Powell and Alley, 1997; Batchelor and Dowdeswell, 2015). Stacked GZWs of similar dimensions and geometry to those in Jason Trough are identified over wider areas of the seafloor on the mid-Norwegian continental shelf (Fig. 4b).

A series of sedimentary wedges is also identified on multi-beam echo-sounder, side-scan sonar and sub-bottom profiler data acquired from Larsen Inlet beneath approximately 520–560 m of water (dive 3; Figs. 1b and 5) (Dowdeswell et al., 2020a). Here, we image five wedges with seaward faces that stand 5–15 m above the surrounding seafloor (Fig. 5c–e). These wedges are interpreted as a complex of stacked GZWs that is orientated transverse to the former ice-flow direction as inferred from elongate streamlined ridges (Fig. 5a and b) (Evans et al., 2005; Dowdeswell et al., 2020a). Bathymetric and sub-bottom profiler data acquired from the RRS *James Clark Ross* in 2002 (Fig. 5a and b) have previously shown the existence of a GZW complex in Larsen Inlet (Fig. 1b) (Evans et al., 2005; Lavoie et al., 2015; Evans and Hogan, 2016; Campo et al., 2017). However, the individual stacked GZWs and subdued forms on their low-gradient surfaces (Fig. 5c) (see Section 4.3) are not readily discernible at the resolution of these ship-acquired data.

Our AUV-derived data show that the steeper, ice-distal margin of the GZWs, which has a gradient of up to 12°, has a sinuous form in plan-view that includes several prominent embayments (Fig. 5c). Sediment lobes up to 2 m thick extend up to 500 m from the break in slope at the base of the ice-distal face of the GZWs (Fig. 5f and g). These lobes are interpreted as debris-flow lobes produced by the remobilisation of deformable sediment that was delivered subglacially to the grounding line (King et al., 1991; Powell and Alley, 1997).

The upper surface of the GZWs in Larsen Inlet is characterised by a high-amplitude irregular reflection on sub-bottom profiles (Fig. 5e). This reflection is typically acoustically impenetrable, although deeper sub-bottom reflections (arrowed in Fig. 5e) are sometimes identified where overlying sediment is thinner. A thin (~1 m) acoustically semi-transparent drape, which is interpreted as glacimarine sediment, overlies the surface of the wedges across the surveyed area (Fig. 5e). This is consistent with geological evidence from a vibrocore (VC318) that was acquired close to the surveyed area (Fig. 5a), which was interpreted to contain 1.2 m of sub-ice shelf to open-marine sediment overlying subglacial diamictic sediment (Evans et al., 2005).

The GZW complexes in Jason Trough and Larsen Inlet (Figs. 3a and 5c) were probably produced during regional deglaciation of the APIS following the LGM. Radiocarbon dates suggest that the GZWs in Larsen Inlet were formed sometime before 10.6 ka (Brachfeld et al., 2003; Evans et al., 2005; Pudsey et al., 2006; Ó Cofaigh et al., 2014), whilst model reconstructions suggest that the surveyed area in Jason Trough became ice free between around 15 and 10 ka (Ó Cofaigh et al., 2014). As the GZWs in Jason Trough and Larsen Inlet are probably of similar age, the significantly thicker drape of glacimarine sediment in Jason Trough (up to 8 m; Fig. 3e and f) compared with that in Larsen Inlet suggests that Jason Trough has experienced higher rates of glacimarine sedimentation since the wedges were formed. Assuming that the surveyed sites in Larsen Inlet and Jason Trough both became free from grounded ice around 10.6 ka (Evans et al., 2005; Ó Cofaigh et al., 2014), the deglacial and Holocene sedimentation rate is more than six times higher in central Jason Trough (~0.75 m per thousand years) compared with in Larsen Inlet (~0.11 m per thousand years). It is possible that Jason Trough has acted as a trap for sediment carried in bottom currents, including sediment winnowed from shallower inter-trough banks (Fig. 1a and c). In contrast, the relatively open bathymetry beyond Larsen Inlet (Fig. 1b) may have encouraged sediment transported within ocean currents to be spread more widely across the shelf.

4.3. Tidal ridges produced along the grounding line – ice-marginal

An assemblage of landforms is preserved on the low-gradient GZW surfaces in Larsen Inlet (Fig. 5c and d). Elongate parallel-to-flow ridges up to 4 m high and spaced 50–200 m apart are overprinted by more

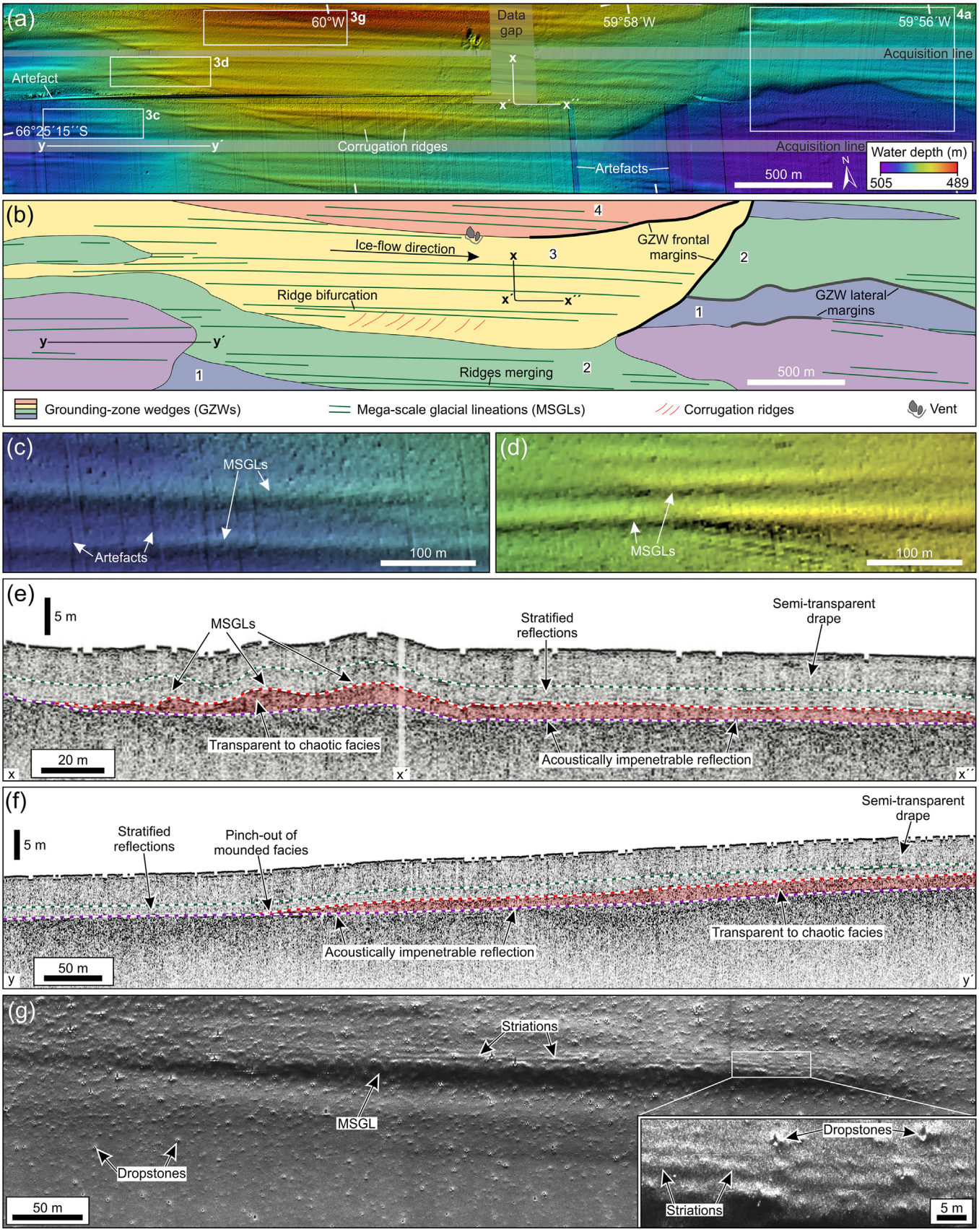

Fig. 3. Geophysical data acquired from central Jason Trough during AUV dive 2 (location in Fig. 1c). (a) HISAS-derived bathymetric data. Grid-cell size 1 m. Grey areas show lines of data acquisition. (b) Interpretation of bathymetric data shown in (a). Numbers are grounding-zone wedge (GZW) surfaces. Thick black and dark grey lines delimit some of the frontal and lateral margins of the GZWs, respectively. (c) and (d) Detail of the mega-scale glacial lineations (MSGLs) in Jason Trough. (e) and (f) Sub-bottom profiles through the near-seafloor sediments in Jason Trough. Profile locations are shown in (a) and (b). Green, red and purple dashed lines mark lower reflections of acoustically transparent, stratified, and transparent to chaotic units, respectively. (g) HISAS amplitude image of MSGLs in Jason Trough. Inset is detail showing striations and large clasts on the seafloor.

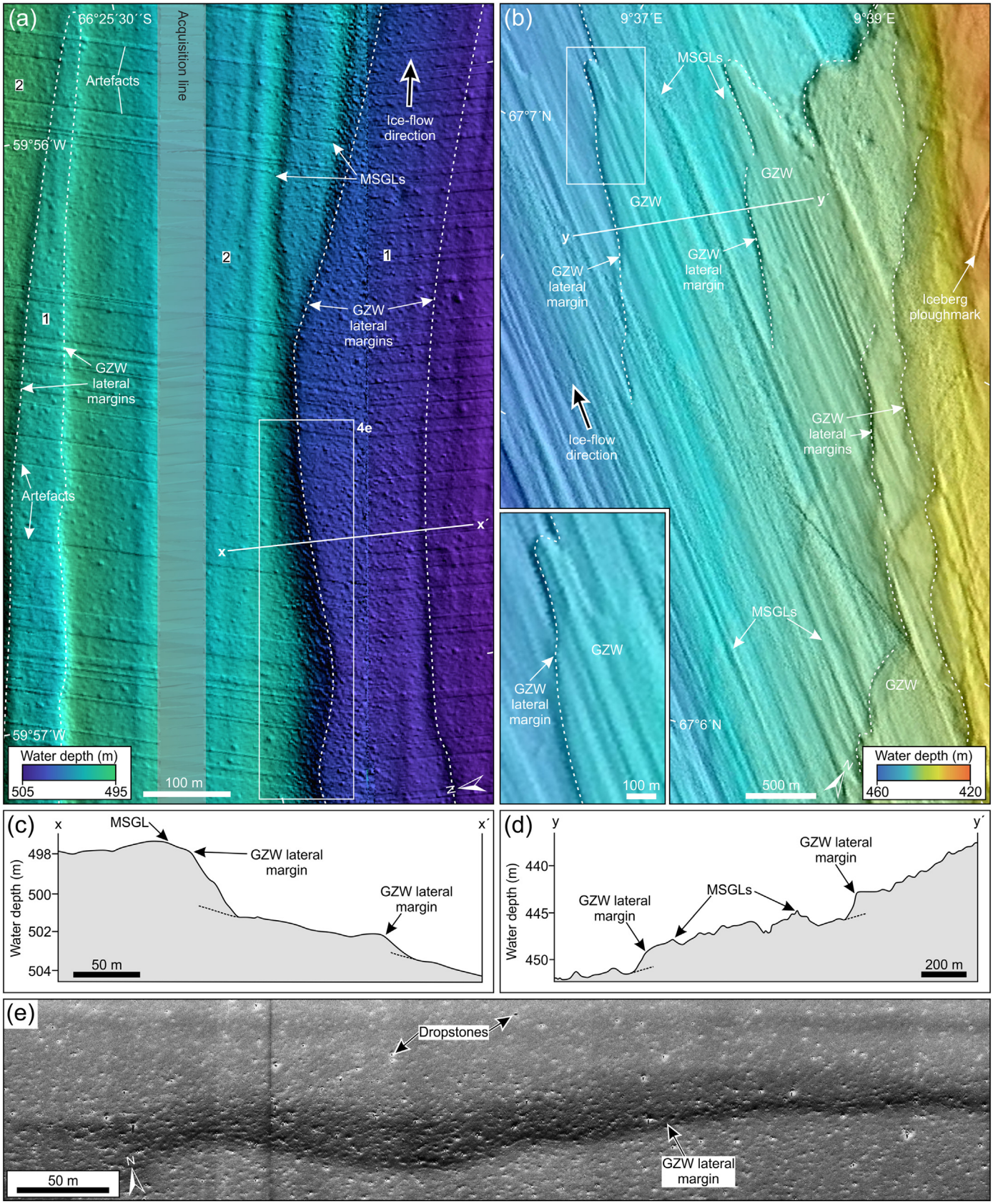

Fig. 4. Examples of sediment wedges, interpreted as small GZWs. (a) Detail of sediment wedges in central Jason Trough. Location is in Fig. 3a. White dashed lines mark the lateral margins of the GZWs. Grid-cell size 1 m. (b) Bathymetric data acquired during the Mareano programme shows similar GZW lateral margins on the continental shelf of mid-Norway. Grid-cell size 5 m. Inset shows part of a GZW lateral margin at the same scale as in (a). (c) and (d) Profiles across the lateral margins of the GZWs in Jason Trough and off mid-Norway, respectively. (e) HISAS imagery of the lateral margin of a GZW in Jason Trough.

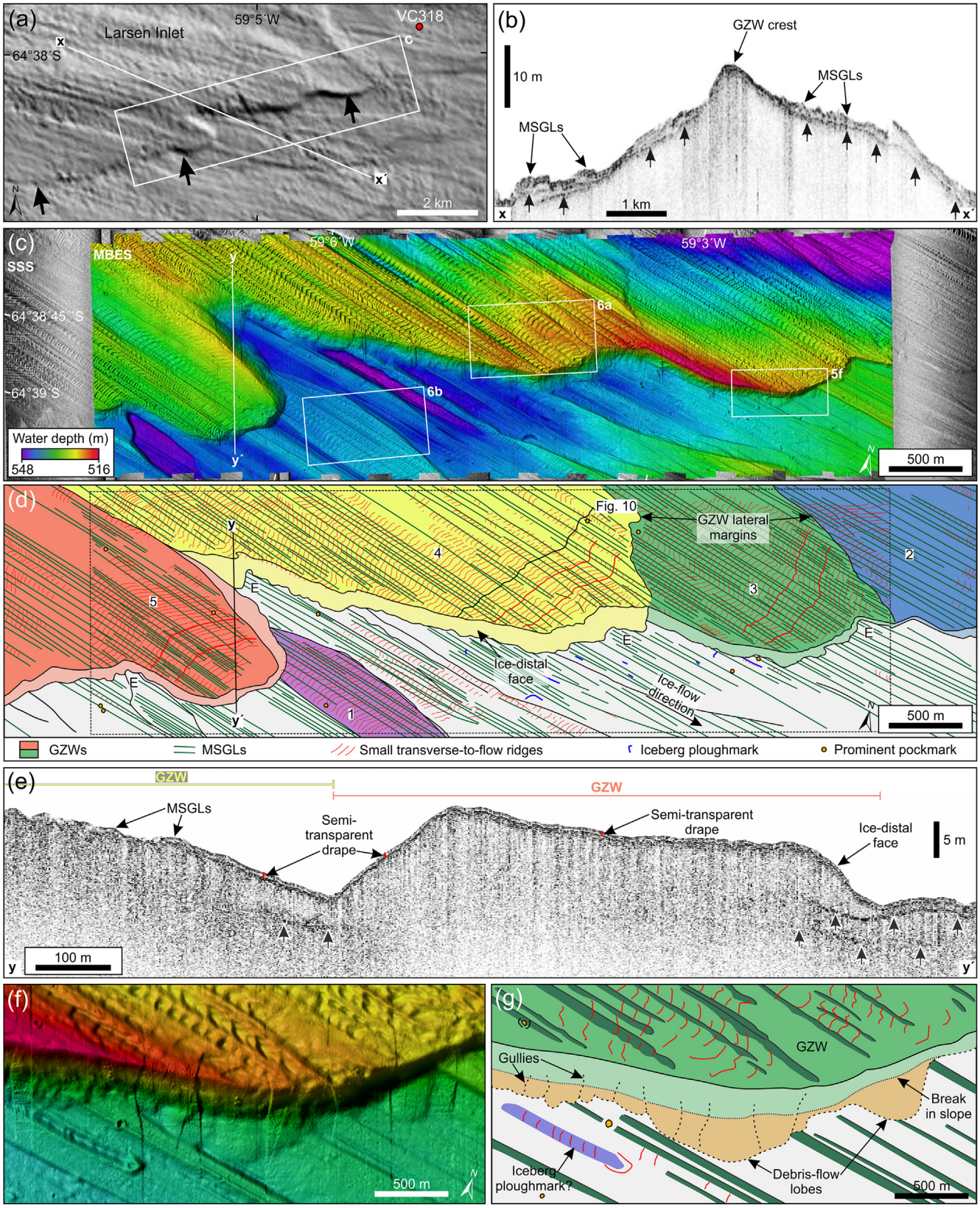

Fig. 5. Geophysical data acquired from Larsen Inlet. (a) Bathymetric data of a GZW complex in Larsen Inlet, acquired from RRS *James Clark Ross* in 2002 using a Kongsberg EM120 multibeam echo-sounder with a frequency of 12 kHz. Grid-cell size 50 m. The image is modified from Evans et al. (2005). Black arrows show GZW crest. Red circle is location of vibrocore VC318. (b) Sub-bottom profile across the GZW, acquired from RRS *James Clark Ross* in 2002 using a Kongsberg TOPAS PS18 sub-bottom profiler with a primary frequency of 3.5 kHz. Arrows mark an acoustically impenetrable reflection at the base of the GZW. The image is modified from Evans et al. (2005). (c) AUV-derived bathymetric (coloured) and side-scan sonar (greyscale) data of the GZW complex in Larsen Inlet, acquired during AUV dive 3 (location in Fig. 1b). Grid-cell size 1 m. (d) Interpretation of the GZW complex shown in (c). Numbers are individual GZW surfaces. E = embayment. (e) AUV-derived sub-bottom profile across GZWs 4 and 5. Profile location is in (c) and (d). Arrows mark subsurface reflections that are interpreted as the bases of the stacked GZWs. (f) Detail of debris-flow lobes on the distal slope of the GZWs. (g) Interpretation of the features shown in (f). Key is the same as in (d).

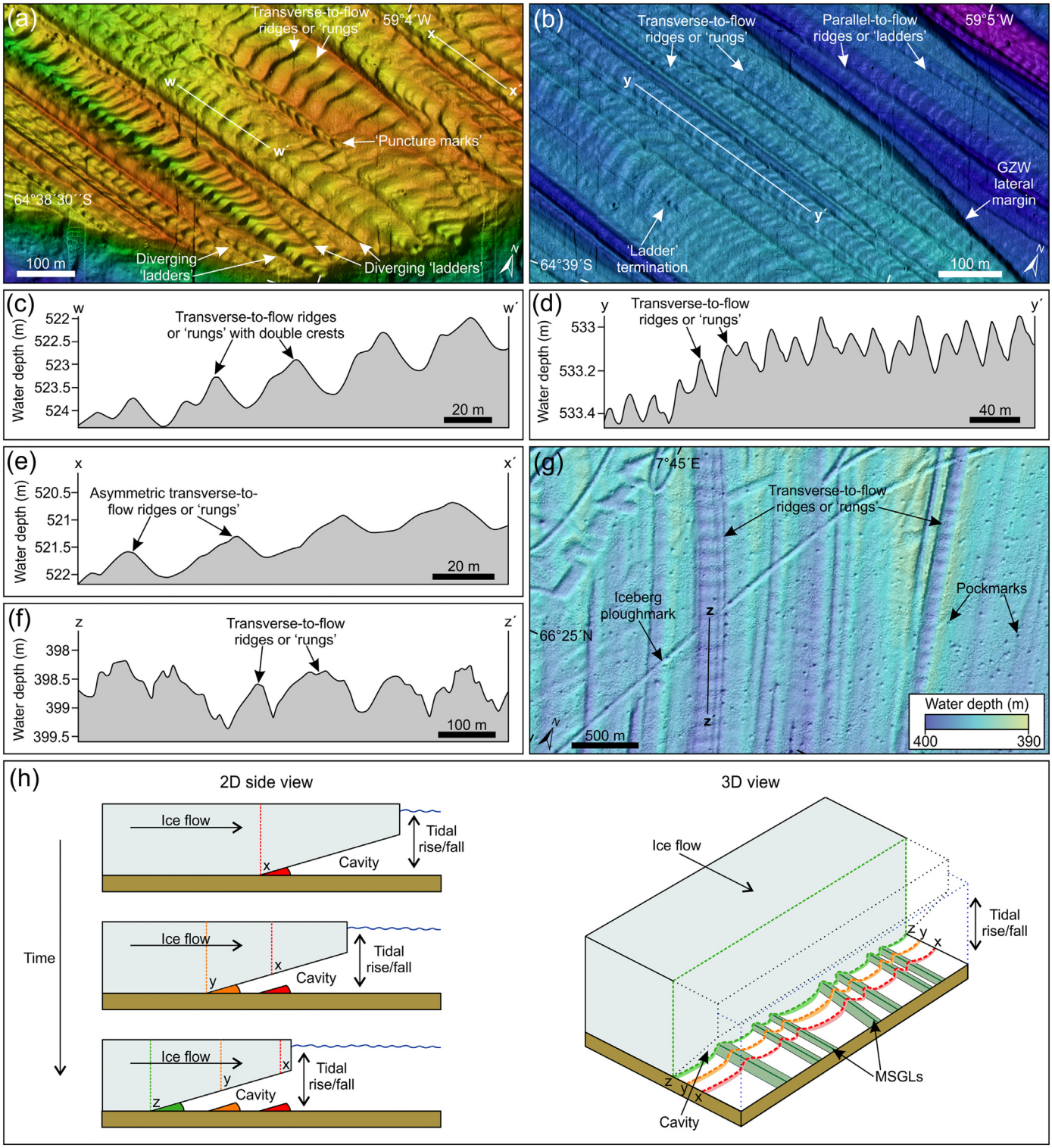

Fig. 6. Detail of 'ladder and rung topography'. (a) and (b) Detail of the delicate assemblage of landforms on the low-gradient upper surface of the GZWs in Larsen Inlet. Locations are in Fig. 5c. (c) to (e) Profiles across select transverse-to-flow ridges or rungs on the GZWs. (f) Profile across the transverse-to-flow ridges on the mid-Norwegian margin, which are shown in (g). (g) Bathymetric data acquired during the Mareano programme showing similar ladder and rung topography on the continental shelf of mid-Norway. Grid-cell size 5 m. (h) Schematic models of the hypothesised formation of transverse-to-flow ridges on the surface of a GZW, which are based on the model proposed in Dowdeswell et al. (2020a). The letters x, y and z show the former position of the retreating grounding line.

than 200 transverse-to-flow ridges that are 0.1–1.5 m high and spaced about 20–40 m apart (Fig. 6a–e). This assemblage has been described previously as 'ladder and rung topography' by Dowdeswell et al. (2020a). In this model, the 'ladders' are MSGLs formed subglacially beneath fast-flowing ice during GZW deposition, and the superimposed 'rungs' are corrugation ridges produced by the squeezing up of soft sediment during tidally induced motion of the grounding line during subsequent grounding-line retreat (Fig. 6h) (Dowdeswell et al., 2020a). Continuous grounding-line retreat is necessary to prevent the ridges from being deformed or eroded during the next tidal cycle.

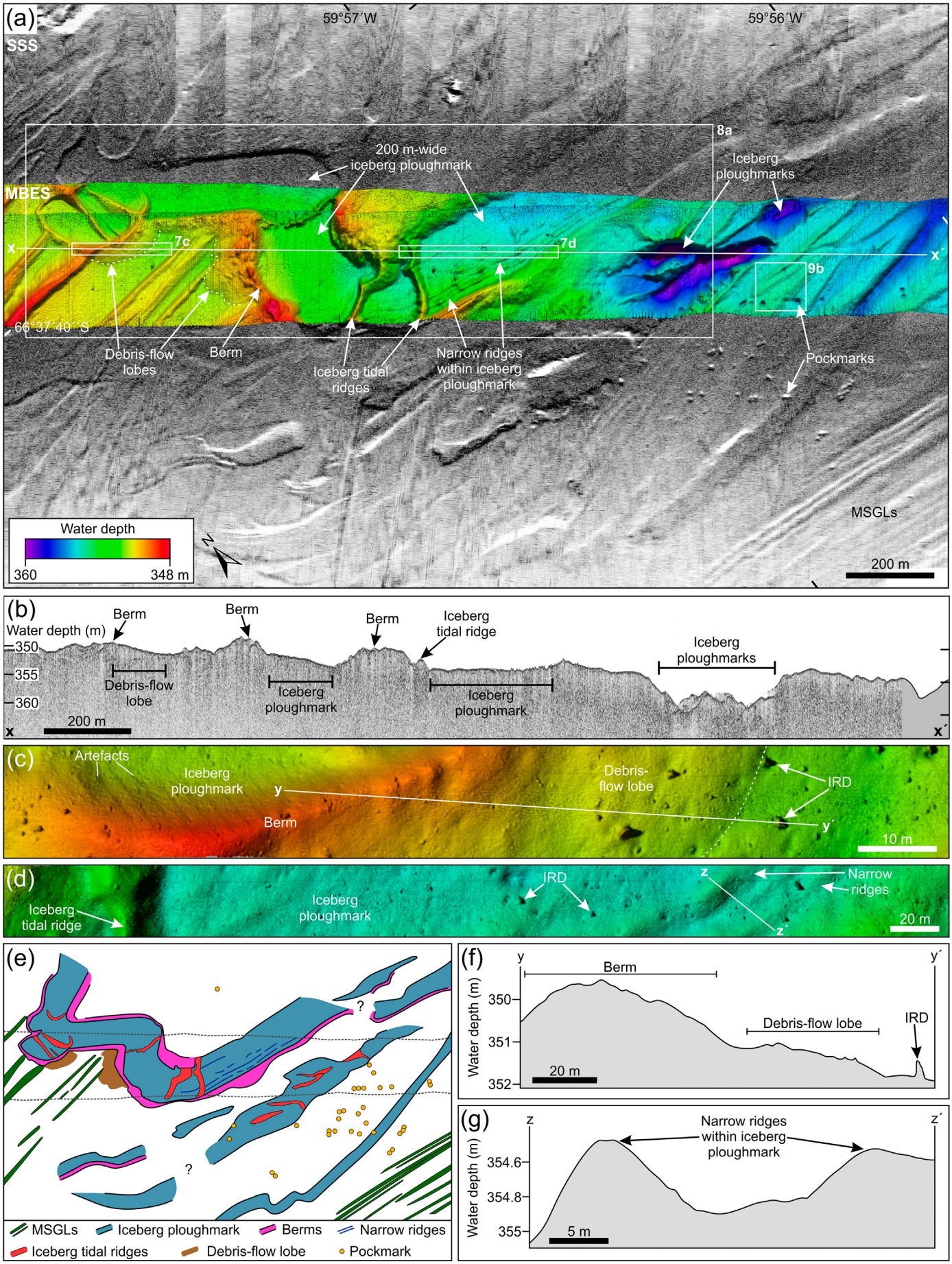
(a)
SSS
59°57´W
59°56´W
8a
200 m-wide iceberg ploughmark
Iceberg ploughmarks
MBES
x
7c
7d
x´
9b
66°37´40´´S
Debris-flow lobes
Berm
Iceberg tidal ridges
Narrow ridges within iceberg ploughmark
Pockmarks
MSGLs
Water depth
360
348 m
200 m
(b)
Water depth (m)
Berm
Berm
Berm
Iceberg tidal ridge
Iceberg ploughmarks
350
355
360
Debris-flow lobe
Iceberg ploughmark
Iceberg ploughmark
200 m
x
x´
(c)
Artefacts
Iceberg ploughmark
y
Berm
Debris-flow lobe
IRD
y´
10 m
(d)
Iceberg tidal ridge
Iceberg ploughmark
IRD
z
Narrow ridges
z´
20 m
(e)
?
?
MSGLs
Iceberg ploughmark
Berms
Narrow ridges
Iceberg tidal ridges
Debris-flow lobe
Pockmark
(f)
y
y´
Berm
Water depth (m)
350
351
352
Debris-flow lobe
IRD
20 m
(g)
z
z´
Narrow ridges within iceberg ploughmark
Water depth (m)
354.6
354.8
355
5 m

Here, we show that, although the irregular, sinuous shape of the corrugation ridges is relatively consistent in the ice-flow direction, there are subtle along-flow variations in their shape and dimensions. For example, distinctive patterns, including near-circular depressions or 'puncture marks' are present over small areas of the seafloor (Fig. 6a). Some MSGLs diverge in the ice-flow direction (Fig. 6a). In other areas, corrugation ridges that were separated by a MSGL ridge become joined in the ice-flow direction when the MSGL ceases to have expression on the seafloor (Fig. 6b). These small-scale variations are interpreted to reflect subtle changes in the shape of the grounding line as the ice flowed forward (Fig. 6h).

The relatively uniform spacing of the corrugation ridges (Figs. 5c, d and 6) implies a consistent rate of grounding-line retreat and the absence of localised longitudinal differences in tidal variability across the surveyed area. Given the rapid rates of grounding-line retreat (up to 50 m/day) inferred from the spacing of the corrugation ridges (cf. Dowdeswell et al., 2020b), we propose that ocean-driven basal melting and consequent ice-shelf thinning was the predominant driver of grounding-line retreat in Larsen Inlet during regional deglaciation, similar to the key mechanism controlling contemporary glacier recession in West Antarctica (Khazendar et al., 2016).

Similar transverse-to-flow corrugation ridges spaced about 50 m apart are identified overprinting a small area (~0.2 km^2) of the GZW surface in Jason Trough (Fig. 3a and b). These features are associated with positive-relief MSGLs, rather than seafloor incisions produced by icebergs or sub-ice shelf keels, and are therefore interpreted to have formed at a retreating ice-sheet grounding line. The subdued seafloor expression of these ridges, which are ~0.3 m high, may be related to the thicker unit of glacimarine sediment that covers the GZW surfaces in this area compared to that in Larsen Inlet (8 m compared with 1 m) (Figs. 3f, g and 5e). Corrugation ridges of similar dimensions and geometry to those identified in Jason Trough and Larsen Inlet are also identified on the mid-Norwegian margin (Fig. 6f and g).

4.4. Iceberg ploughmarks - proglacial

Linear to curvilinear depressions up to 5 m deep are identified on multibeam echo-sounder, side-scan sonar and sub-bottom profiler data from the southern lateral margin of Jason Trough (dive 1; Figs. 1c and 7). These depressions are interpreted as iceberg ploughmarks formed by the grounding of iceberg keels in soft seafloor sediments (e.g. Woodworth-Lynas et al., 1991; Dowdeswell et al., 1993; Metz et al., 2008; Wise et al., 2017). The width and U-shaped geometry of a prominent 200 m-wide ploughmark in the surveyed area (Fig. 7a), along with the water depth of approximately 350 m, suggests that it was produced by a tabular iceberg that calved from an ice shelf (e.g. Dowdeswell and Bamber, 2007). Iceberg ploughmarks of similar dimensions and geometry have been mapped at coarser resolution on conventional multibeam echo-sounder data collected from beyond Larsen C Ice Shelf (Dowdeswell et al., 2020a).

AUV-derived multibeam echo-sounder data acquired from a height of 10 m show numerous clasts up to 1 m high on or close to the seafloor (Fig. 7c and d), which are interpreted as IRD. Our AUV-derived data also reveal three different types of delicate ridges associated with the 200 m-wide iceberg ploughmark. First, elongate ridges up to 3 m high are identified along both ploughmark flanks (Fig. 7a, c and e). These ridges are interpreted as berms formed by the relocation of sediment as the iceberg keel incised the seafloor. The pushing of seafloor sediments by iceberg keels can cause small-scale sediment failures on the distal sides of berms (Lien et al., 1989; Woodworth-Lynas et al., 1991; Linch et al., 2012), as shown here by the subdued debris-flow lobes that extend up to 100 m beyond the berms (Fig. 7c and f). Secondly, subdued linear ridges that are ~10 m wide and 0.5 m high are present within and aligned parallel to the central depression (Fig. 7a, d and g). These narrow ridges were probably formed by variations in the basal roughness of the iceberg keel.

Finally, irregularly spaced ridges up to 2 m high and 20–40 m wide extend across the full width of the 200 m-wide iceberg ploughmark (Figs. 7a, e and 8). These relatively high-amplitude ridges have an arcuate shape in plan-view (Fig. 8a) and an asymmetric cross-profile in which the seafloor deepens beyond their slightly steeper side (Fig. 8c). They are interpreted to have been produced when the iceberg was lowered and/or moved backwards under a falling tide, which pushed up a ridge of sediment behind the iceberg keel, before it continued on its original trajectory with the rising tide. A schematic model for the formation of these iceberg tidal ridges is presented in Fig. 8e. The preservation of the tidal ridges, which do not show any evidence of subsequent erosion or disturbance, suggests that they were not formed by the pushing-up of sediment in the overall direction of iceberg drift. Even if the keel of an iceberg was able to clear a ridge of sediment that it had produced in front of it, for example during the rising tide, the area of seafloor immediately in front of the ridge would not be eroded by the iceberg keel; this process may, instead, explain the formation of iceberg pits that are separated by non-ploughed areas of the seafloor, which are common features on glaciated margins (e.g. Fig. 8b).

Ridges that extend across the width of iceberg ploughmarks are also identified on bathymetric data from the mid-Norwegian margin (Fig. 8b). These ridges are up to 3 m high and display the same arcuate plan-view shape and asymmetric cross-sectional geometry as the ridges on the NE Antarctic Peninsula shelf (Fig. 8a–d). The iceberg tidal ridges that we image at the southern lateral margin of Jason Trough and on the mid-Norwegian shelf (Fig. 8) have steeper sides and are less regularly spaced than subdued ridges that have been identified previously within iceberg ploughmarks and referred to as washboard patterns or corrugation ridges (Barnes and Lien, 1988; Lien et al., 1989; Jakobsson et al., 2011; Jakobsson and Anderson, 2016; Dowdeswell and Hogan, 2016).

5. Discussion

The horizontal resolution of the bathymetric data acquired from our AUV surveys on the NE Antarctic Peninsula continental shelf, which ranges from 0.1 to 0.5 m (Figs. 3–7), is an order of magnitude higher than the resolution of the majority of data acquired from conventional hull-mounted multibeam echo-sounders, which is usually at least a few metres (e.g. Dowdeswell et al., 2004; Evans et al., 2006; Livingstone et al., 2016; Larter et al., 2019). This enables the identification of subdued seafloor features, including corrugation ridges and small GZWs, and permits new insights into the formation of submarine glacial landforms.

5.1. Tidally influenced glacial landforms

Our high-resolution bathymetric data enable features produced by the tidally influenced motion of ice to be identified clearly on the seafloor. Transverse-to-flow ridges interpreted to have been produced by the interaction of ice and tides have been reported on several Antarctic continental shelves, where they have been referred to as corrugation ridges (Jakobsson et al., 2011; Graham et al., 2013; Klages et al., 2015; Halberstadt et al., 2016; Jakobsson and Anderson, 2016; Smith et al., 2019). There are three mechanisms by which corrugation ridges can be

Fig. 7. Geophysical data acquired from the southern lateral margin of Jason Trough during AUV dive 1 (location in Fig. 1c). (a) AUV-derived multibeam echo-sounder (coloured) and side-scan sonar (greyscale) data, showing a 200 m-wide iceberg ploughmark and associated features. Grid-cell size 1 m. (b) Sub-bottom profile along the bathymetric data shown in (a). (c) and (d) Detail of the subdued features associated with the iceberg ploughmark. Grid-cell size 0.2 m. (e) Interpretation of glacial landforms from the bathymetric data shown in (a). (f) and (g) Profiles across the subdued features associated with iceberg ploughmarks. Locations are in (c) and (d).

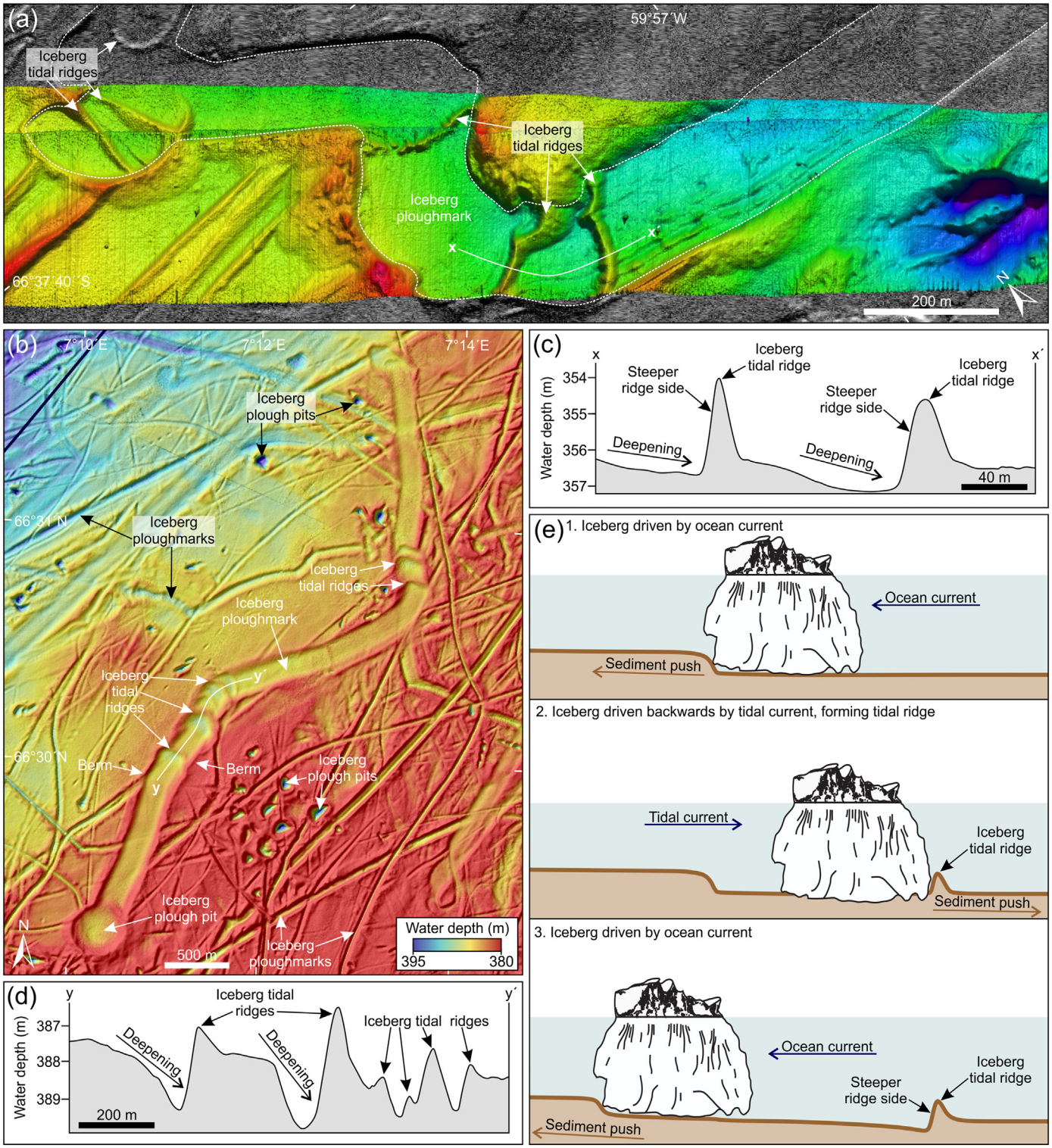

Fig. 8. Detail of iceberg tidal ridges. (a) Iceberg tidal ridges at the southern lateral margin of Jason Trough. Location in Fig. 7a. (b) Bathymetric data acquired during the Mareano programme shows similar iceberg tidal ridges on the mid-Norwegian margin. Grid-cell size 5 m. (c) and (d) Profiles across the iceberg tidal ridges at the southern lateral margin of Jason Trough and on the mid-Norwegian margin, respectively. The iceberg tidal ridges are asymmetric with a deeper area of seafloor immediately beyond one side of each ridge. (e) Schematic models of the hypothesised formation of iceberg tidal ridges.

produced in glacier-influenced environments (cf. Jakobsson et al., 2011; Graham et al., 2013; Supplementary Table 1 in Dowdeswell et al., 2020a). First, the squeezing up of soft seafloor sediments by the vertical motion of the ice-sheet grounding line during tidal cycles can produce regularly spaced transverse-to-flow ridges which are preserved when the grounding line is undergoing retreat (Figs. 6 and 9a) (Dowdeswell et al., 2020a). These features are smaller and more regularly spaced than push moraines that form, often annually, during short-lived re-advances during general grounding-line retreat (Boulton, 1986; Ottesen and Dowdeswell, 2006; Burton et al., 2016; Batchelor et al., 2019b). Secondly, it is possible that the tidally influenced grounding of sub-ice shelf keels can produce subdued ridges within incisions that are interpreted

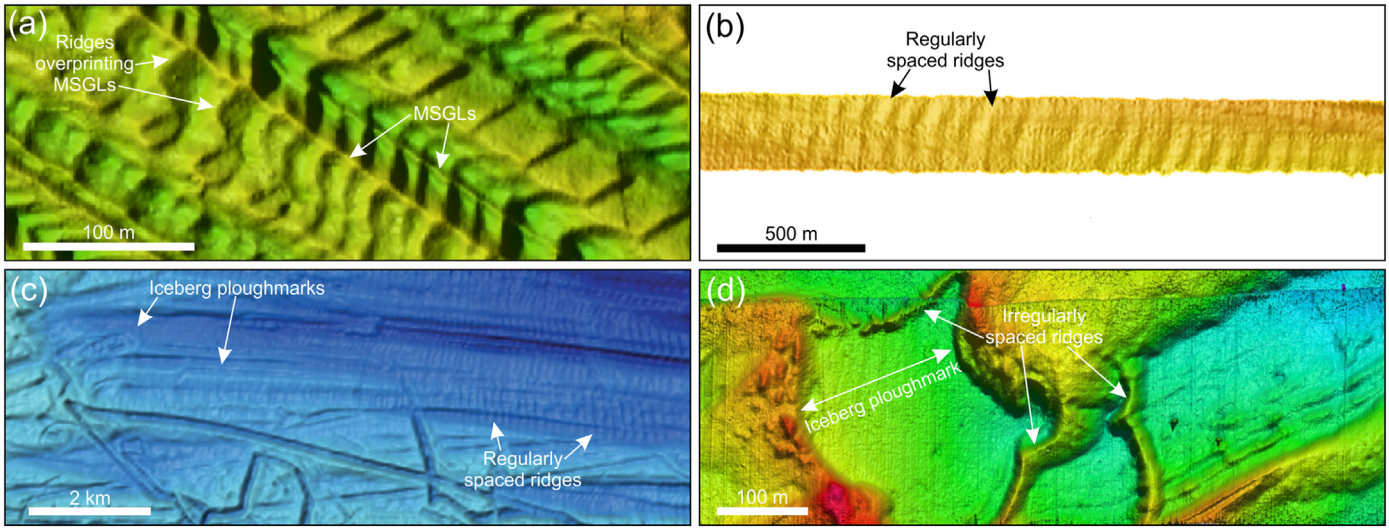

Fig. 9. Examples of subdued ridges interpreted to have been produced by the interaction of ice and tides (corrugation ridges) on Antarctic continental shelves. (a) Detail of the transverse-to-flow ridges in Larsen Inlet, which are interpreted to have been produced along the ice-sheet grounding line (Dowdeswell et al., 2020a). Note that the ridges overprint linear features interpreted as MSGLs. (b) Regularly spaced ridges on the seafloor beneath Pine Island Glacier Ice Shelf, which have been interpreted to have been formed by the tidally influenced motion of sub-ice shelf keels close to the grounding line (adapted from Graham et al. (2013)). (c) Regularly spaced ridges within parallel iceberg ploughmarks in Pine Island Bay, West Antarctica (adapted from Jakobsson and Anderson (2016)). (d) Irregularly spaced ridges within an iceberg ploughmark at the southern lateral margin of Jason Trough.

as sub-ice shelf keel scours (Fig. 9b) (Graham et al., 2013; Smith et al., 2019). Thirdly, the tidal-driven motion of grounded or near-grounded icebergs can produce ridges of soft seafloor sediments within iceberg ploughmarks (Figs. 8, 9c and d) (Barnes and Lien, 1988; Lien et al., 1989; Jakobsson et al., 2011; Smith et al., 2019). Regularly spaced iceberg tidal ridges (Fig. 9c) are probably produced when icebergs are trapped within mélange (a frozen mix of sea-ice floes and small bergy bits) (e.g. Jakobsson et al., 2011), whilst irregularly spaced ridges (Figs. 8 and 9d) are formed when the tidally influenced grounding and ungrounding of icebergs occurs in relatively open water. The presence of iceberg tidal ridges on the Norwegian continental margin (Figs. 6g and 8b) shows that these seafloor features are not unique to Antarctica; they are probably relatively widespread on formerly glaciated margins, but often require very high-resolution bathymetric data to be identified clearly.

It is important to differentiate between tidal ridges that are produced by ice in different process environments (i.e. ice-marginal or proglacial). For example, if a recently exposed area of the seafloor that was previously covered by a floating ice shelf is heavily scoured by iceberg ploughmarks, the calving margin of the ice shelf can be assumed to have been landward of this region in the relatively recent past (e.g. Jakobsson et al., 2011; Graham et al., 2013). Because corrugation ridges produced at the grounding line, by sub-ice shelf keels and by icebergs have broadly similar dimensions and geometries (Fig. 9) (Jakobsson et al., 2011; Graham et al., 2013; Smith et al., 2019; Supplementary Table 1 in Dowdeswell et al., 2020a), the wider geomorphological context and relationship of the ridges with other glacial landforms is essential for interpreting the likely mechanism of corrugation-ridge formation. For example, the grounding-line tidal ridges in Larsen Inlet are present over a wide (up to at least 9 km^2) region of the seafloor where they overprint MSGLs and the low-gradient ice-proximal sides of GZWs (Figs. 5 and 6), whereas iceberg tidal ridges are confined within iceberg ploughmarks (Figs. 8 and 9). However, it is not always possible to examine the wider

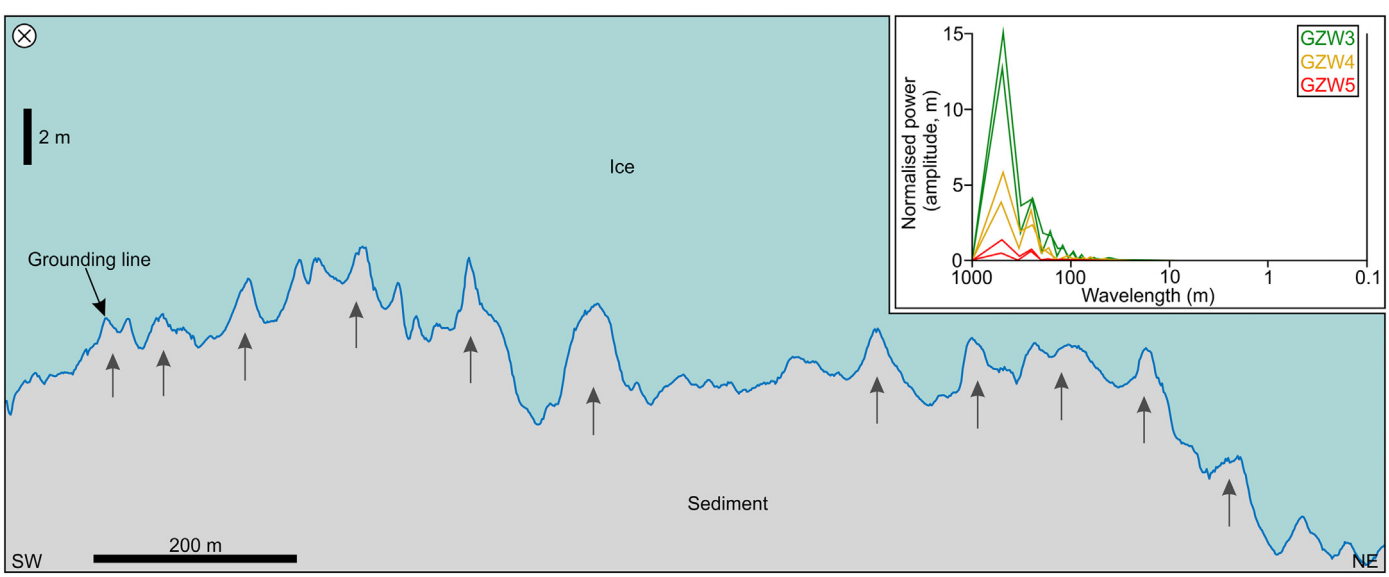

Fig. 10. Profile showing the roughness of the ice-bed interface at a former grounding line position in Larsen Inlet. Location of the profile is shown by the black line in Fig. 5d. Grey arrows are seafloor MSGLs. Inset is ice sheet basal roughness inferred from power spectra of grounding line vertical profiles following the approach of Taylor et al. (2004). The selected six former grounding line positions are shown by thick red lines in Fig. 5d. Variation in power (equivalent of amplitude, m) is shown with respect to wavelength (m) on a logarithmic scale.

geomorphological context of subdued ridges preserved on the seafloor, particularly when interpreting AUV-derived data of relatively low spatial coverage and especially where only single tracks are available.

The identification of corrugation ridges produced along a former grounding line (Fig. 6) has implications for ice sheet reconstruction. First, these ridges enable the rate of grounding-line retreat to be estimated, using the assumption that two ridges are produced each day from two tidal cycles (Dowdeswell et al., 2020a). Secondly, laterally continuous grounding-line tidal ridges reveal the shape of the former grounding line and ice sheet base. In the transverse-to-flow direction, along the former grounding line (thick red lines in Fig. 5d), variations in seafloor topography occur at wavelengths of between 100 and 1000 m, with a peak at around 200 m (Fig. 10). These wavelengths mainly reflect the spacing of MSGLs on the seafloor. Along-flow variations in the morphology of grounding-line tidal ridges, including the widening of ladders and development of 'puncture marks' (Fig. 6a and b), are interpreted to reflect small-scale variations in the along-flow shape of the ice sheet base, which led to subtle changes in the shape of the grounding line as the ice flowed forward (Fig. 6h). In Larsen Inlet, the shape of the former ice sheet base appears to have been variable in the across-flow direction (Fig. 10) yet relatively consistent in the along-flow direction over a scale of several kilometres (Fig. 5c). Information about the roughness of the ice sheet base is important for explaining the formation of elongate subglacial landforms (Clark et al., 2003; King et al., 2009; Stokes et al., 2013; Spagnolo et al., 2014) and for estimating basal melting in numerical ice sheet models (Taylor et al., 2004; Buchardt and Dahl-Jensen, 2007; Gwyther et al., 2015).

The asymmetry of irregularly spaced corrugation ridges preserved within iceberg ploughmarks (Fig. 8c and d) enables the overall drift direction of former icebergs to be reconstructed. The iceberg ploughmark at the southern lateral margin of Jason Trough (Figs. 7a and 8a) is interpreted to have been drifting in a generally westerly direction, which is consistent with the trajectory of modern-day icebergs and the clockwise circulation of the Weddell Gyre (Deacon, 1979; Muench and Gordon, 1995). The asymmetry of the iceberg tidal ridges in the example off mid-Norway (Fig. 8d) suggests that the iceberg which formed the ploughmark drifted in a generally southerly direction before grounding more firmly on the shallower seafloor to the south, forming a large iceberg plough pit, prior to melting and/or rotating (Fig. 8b). When applied to numerous iceberg ploughmarks, this information could be used to reconstruct the direction of past ocean currents (Todd et al., 1988; Schodlok et al., 2006; Newton et al., 2016; Montelli et al., 2018).

5.2. A continuum of grounding line depocentres

Another consequence of our high-resolution data is that morphologically subdued depocentres that built up at the former ice-sheet grounding line can be identified on the seafloor (Figs. 4a, e and 5c). We recognise two different scales of grounding line depocentres. First, and the smaller of the two, corrugation ridges with heights of 0.1–1.5 m and along-flow lengths of 20–40 m (Fig. 6a and b) are interpreted to be formed by the tidal-driven motion of the grounding line during successive tidal cycles (Fig. 6h). These subdued ridges are formed over short temporal timescales (twice daily) and record the former grounding line position (Dowdeswell et al., 2020a).

Secondly, and significantly larger than the tidal ridges produced along the former grounding line, relatively small GZWs (Fig. 4a, e and 5c) with estimated volumes of less than 0.5 km^3 are identified in Jason Trough and Larsen Inlet (Figs. 3a, 4c, 5c and e). These landforms are interpreted to have been produced by sediment delivery to the grounding line when it remained in a broadly similar position over a timescale of years to perhaps a few decades. These sedimentary depocentres have similar dimensions to other small GZWs identified in the geological record, including on the western Ross Sea continental shelf, Antarctica (Simkins et al., 2017, 2018).

Although the GZWs in Jason Trough and Larsen Inlet probably extend beyond the surveyed areas, they are smaller than most of the GZWs that have been mapped previously on mid- and high-latitude continental margins, which have typical volumes of between ten and several hundred cubic kilometres (Anderson, 1997; O'Brien et al., 1999; Ó Cofaigh et al., 2005; Ottesen et al., 2007; Dowdeswell and Fugelli, 2012; Rydningen et al., 2013; Batchelor and Dowdeswell, 2015). Our limited knowledge of sediment fluxes beneath present-day fast-flowing outlet glaciers suggests that GZWs of these dimensions are probably produced during ice-marginal still-stands of at least several decades to centuries (Larter and Vanneste, 1995; Alley et al., 2007; Anandakrishnan et al., 2007; Dowdeswell et al., 2008a). The relative absence of reports of small GZWs in the marine geological record is probably because most ship-based geophysical surveys, which typically acquire bathymetric data with a horizonal resolution of at least several metres, are often only able to image larger GZWs that indicate longer-term grounding-zone stability. The presence of small GZWs suggests that the grounding line of ice sheets that transition into an ice shelf can be sensitive to short-term mass balance fluctuations. This is in agreement with recent studies of satellite data showing inter-decadal changes in the position of the grounding line landward of Antarctic ice shelves (Rignot et al., 2014, 2019; Christie et al., 2016, 2018; Khazendar et al., 2016; Scheuchl et al., 2016).

The small GZWs imaged in Larsen Inlet (Fig. 5c) are part of a wider GZW complex that records a period of relative grounding-zone stability during the last deglaciation, which was probably encouraged by the narrowing of the continental shelf between Cape Longing and Cape Sobral (Fig. 1b) (Evans et al., 2005). It is likely that other large GZWs on formerly glaciated margins also comprise multiple smaller, partially overlapping wedges (e.g. Dowdeswell and Ottesen, 2016; Bart et al., 2017) that were formed during small-scale fluctuations of the ice-sheet grounding zone occurring within a broader period of relative grounding-zone stability.

5.3. Patterns and processes of glacier-influenced sedimentation

Our AUV-derived data enable insights into the processes by which glacial landforms are produced. Meltwater channels have previously been identified extending from the distal sides of GZWs on the western Ross Sea continental shelf, Antarctica (Simkins et al., 2017, 2018) and occasionally within buried GZWs on the continental shelf of Greenland (Dowdeswell and Fugelli, 2012). Channel-fan complexes have also been imaged on the ice-distal slopes of GZWs on the mid-Norwegian and western Barents Sea margins (Bjarnadóttir et al., 2013; Montelli et al., 2017). A link between the locations of subglacial meltwater channels and embayments in the frontal margin of GZWs has been suggested, with embayments developing as a result of enhanced sediment transport by meltwater or reduced transport of subglacial sediment due to porewater drainage (Simkins et al., 2018).

No evidence of channelised meltwater is identified from the surveyed areas in Jason Trough and Larsen Inlet despite the high-resolution data (Figs. 4e and 5c) and the draping of the uppermost GZW surface in Larsen Inlet with only a thin (~1 m) unit of glacimarine sediment (Fig. 5e). Instead, the ice-distal margins of these GZWs are characterised by debris-flow lobes (Fig. 5f and g), which are interpreted to have been produced by the remobilisation of deformable sediment that was delivered to the grounding line by basal flowage from up-glacier (King et al., 1991; Powell and Alley, 1997). The lack of geophysical evidence of channelised meltwater in our study areas is supported by the general absence of meltwater-derived facies from a vibrocore (VC318) acquired from Larsen Inlet (Fig. 5a) (Evans et al., 2005). Although channelised meltwater is clearly important in the formation of some GZWs, particularly in relatively warmer glacier-influenced marine environments or in areas of high geothermal heat flux (Bjarnadóttir et al., 2013; Simkins et al., 2017, 2018), it appears not to be essential for GZW formation. The acoustically chaotic character of many GZWs on seismic records, and a general absence of internal laminations, also suggests that the delivery of diamictic sediment to the grounding line is the dominant process in

the formation of most GZWs (Anderson, 1997; Bart and Anderson, 1997; O'Brien et al., 1999; Batchelor and Dowdeswell, 2015).

The MSGLs in Jason Trough appear clearly as positive-relief features on our AUV-derived bathymetry and sub-bottom profiles (Fig. 3). The seaward and landward ends of the MSGLs are not associated with any obstacles or recognisable change in substrate (Fig. 3g) that could have encouraged their formation. There is no evidence for free-flowing meltwater (e.g. Shaw et al., 2008), despite the very high-resolution (~0.05 m) of the HISAS images (Fig. 3g). The continuous and flat-lying nature of the basal reflection of the acoustically chaotic to transparent layer of sediment in which the MSGLs are formed (Fig. 3e) implies that continuous plastic deformation of sediment (e.g. Spagnolo et al., 2016), rather than groove-ploughing of the substrate (e.g. Clark et al., 2003), was the main mechanism for the formation of these ridges (Evans et al., 2006; Ó Cofaigh et al., 2007). The bifurcating and merging of the MSGLs (Fig. 3b) support the view that elongate bedforms are continuously produced, remoulded and destroyed beneath fast-flowing ice streams, with remotely sensed observations providing a snapshot of a dynamic sedimentary environment (King et al., 2009; Stokes et al., 2013). It is possible that the narrow (1–2 m wide) elongate ridges that are identified along the crests of some of the MSGLs in Jason Trough ('striations' in Fig. 3g) are incipient MSGLs that would have eventually grown and merged with existing MSGLs, or formed new MSGLs, as underlying features were progressively destroyed.

6. Conclusions

We used AUVs to acquire high-resolution geophysical data from three sites on the NE Antarctic Peninsula continental shelf. AUV-derived multibeam echo-sounder, side-scan sonar, sub-bottom profiler and HISAS data revealed the subdued features associated with subglacially formed MSGLs, ice-marginal GZWs and proglacial iceberg ploughmarks at unprecedented resolution (horizontal resolution of ~0.05 to 0.5 m). Two different types of tidally influenced features are interpreted from these data: 1) regularly spaced grounding-line tidal ridges interpreted to form when soft seafloor sediments are squeezed up by the vertical motion of the ice-sheet grounding line during tidal cycles, and 2) irregularly spaced iceberg tidal ridges formed by the tidally influenced motion of a grounded or near-grounded iceberg. The identification and differentiation of these landforms has implications for revealing past ice dynamics, including estimating the rate of grounding-line retreat, revealing the former shape of the ice sheet base, and estimating the past drift direction of icebergs. The resolution of our AUV-derived data also enables the identification of small GZWs that record relatively short-term, probably annual to decadal, changes in the position of the ice-sheet grounding zone. The absence of evidence for channels associated with these GZWs suggests that channelised meltwater is not essential for GZW formation. Further examples of the delicate features described in this study will be identified as increasingly high-resolution marine-geophysical data are acquired from glaciated continental margins using high-frequency sonar on AUVs and surface vessels.

Declaration of competing interest

The authors declare that they have no known competing financial interests or personal relationships that could have appeared to influence the work reported in this paper.

Acknowledgements

This research was funded by the Flotilla Foundation and Marine Archaeology Consultants Switzerland. The AUVs, associated technical support and initial data pre-processing were provided by Ocean Infinity and Deep Ocean Search. AUV deployments were from the South African icebreaking research vessel SA *Agulhas II*, and we thank the Captain, Ice Pilot, Officers and Crew for their support of our research. We thank the Mareano programme (www.mareano.no) for access to bathymetric data from the Norwegian margin. ESA/Copernicus Sentinel-1a/b Interferometric Wide swath imagery used to map the position of the 2019 ice front was acquired free-of-charge from the Alaskan Satellite Facility (https://search.asf.alaska.edu/#/) in ground range detected (GRD) format. CLB was funded by a Norwegian VISTA post-doctoral scholarship during this work, and FDWC was supported by the Prince Albert II of Monaco Foundation. We thank Johann P. Klages and an anonymous reviewer for their helpful reviews of this paper.

Data availability

Data are available upon request to the authors.

References

Adusumilli, S., Fricker, H.A., Siegfried, M.R., Padman, L., Paolo, F.S., Ligtenberg, S.R.M., 2018. Variable basal melt rates of Antarctic Peninsula ice shelves, 1994–2016. Geophys. Res. Lett. 45, 4086–4095.

Alley, R.B., Anandakrishnan, S., Dupont, T.K., Parizek, B.R., Pollard, D., 2007. Effect of sedimentation on ice-sheet grounding-line stability. Science 315, 1838–1841.

Anandakrishnan, S., Catania, G.A., Alley, R.B., Horgan, H.J., 2007. Discovery of till deposition at the grounding line of Whillans Ice Stream. Science 315, 1835–1838.

Anderson, J.B., 1997. Grounding zone wedges on the Antarctic Continental Shelf, Weddell Sea. In: Davies, T.A., Bell, T., Cooper, A.K., Josenhans, H., Polyak, L., Solheim, A., Stoker, M.S., Stravers, J.A. (Eds.), Glaciated Continental Margins: An Atlas of Acoustic Images. Chapman & Hall, London, pp. 98–99.

Anderson, J.B., 1999. Antarctic Marine Geology. Cambridge University Press, Cambridge, MA.

Anderson, J.B., Shipp, S.S., Lowe, A.L., Wellner, J.S., Mosola, A.B., 2002. The Antarctic Ice Sheet during the Last Glacial Maximum and its subsequence retreat history: a review. Quat. Sci. Rev. 21, 49–70.

Arndt, J.E., et al., 2013. The International Bathymetric Chart of the Southern Ocean (IBCSO) version 1.0 – a new bathymetric compilation covering circum-Antarctic waters. Geophys. Res. Lett. 40, 3111–3117.

Barnes, P.W., Lien, R., 1988. Icebergs rework shelf sediments to 500 m off Antarctica. Geology 16, 1130–1133.

Bart, P.J., Anderson, J.B., 1997. Grounding zone wedges of the Antarctic continental shelf, Antarctic Peninsula. In: Davies, T.A., Bell, T., Cooper, A.K., Josenhans, H., Polyak, L., Solheim, A., Stoker, M.S., Stravers, J.A. (Eds.), Glaciated Continental Margins: An Atlas of Acoustic Images. Chapman and Hall, London.

Bart, P.F., Anderson, J.B., Nitsche, F., 2017. Post-LGM grounding-line positions of the Bindschadler Paleo Ice Stream in the Ross Sea Embayment, Antarctica. Journal of Geophysical Research: Earth Surface 122, 1827–1844.

Batchelor, C.L., Dowdeswell, J.A., 2015. Ice-sheet grounding-zone wedges (GZWs) on high-latitude continental margins. Mar. Geol. 363, 65–92.

Batchelor, C.L., Dowdeswell, J.A., Hogan, K.A., Larter, R.D., Parsons, E., West, O., 2019b. Processes and patterns of glacier-influenced sedimentation and recent tidewater glacier dynamics in Darbel Bay, western Antarctic Peninsula. Antarct. Sci. 31, 218–227.

Batchelor, C.L., Margold, M., Krapp, M., Murton, D.K., Dalton, A.S., Gibbard, P.L., Stokes, C.R., Murton, J.B., Manica, A., 2019a. The configuration of Northern Hemisphere ice sheets through the Quaternary. Nat. Commun. 10, 3713.

Bates, C.R., Lawrence, M., Dean, M., Robertson, P., 2011. Geophysical methods for wreck's site monitoring: the Rapid Archaeological Site Surveying and Evaluation (RASSE) programme. Int. J. Naut. Archaeol. 40, 404–416.

Bentley, M.J., Anderson, J.B., 1998. Glacial and marine geological evidence for the ice sheet configuration in the Weddell Sea-Antarctic Peninsula region during the LGM. Antarct. Sci. 10, 309–325.

Bingham, B., Foley, B., Singh, H., Camilli, R., Delaporta, K., Eustice, R., Mallios, A., Mindell, D., Roman, C., Sakellariou, D., 2010. Robotic tools for deep water archaeology: surveying an ancient shipwreck with an autonomous underwater vehicle. Journal of Field Robotics 27, 702–717.

Bjarnadóttir, L.R., Rüther, D.C., Winsborrow, M.C.M., Andreassen, K., 2013. Grounding-line dynamics during the last deglaciation of Kveithola, W Barents Sea, as revealed by seabed geomorphology and shallow seismic stratigraphy. Boreas 42, 84–107.

Boulton, G.S., 1986. Push-moraines and glacier-contact fans in marine and terrestrial environments. Sedimentology 33, 677–698.

Brachfeld, S., Domack, E., Kissel, C., Laj, C., Leventer, A., Ishman, S., Gilbert, R., Camerlenghi, A., Eglinton, L.B., 2003. Holocene history of the Larsen-a Ice Shelf constrained by geomagnetic paleointensity dating. Geology 31, 749–752.

Buchardt, S., Dahl-Jensen, D., 2007. Estimating the basal melt rate at NorthGRIP using a Monte Carlo technique. Ann. Glaciol. 45, 137–142.

Burton, D.J., Dowdeswell, J.A., Hogan, K.A., Noormets, R., 2016. Little Ice Age terminal and retreat moraines in Kollerfjorden, NW Spitsbergen. In: Dowdeswell, J.A., Canals, M., Jakobsson, M., Todd, B.J., Dowdeswell, E.K., Hogan, K.A. (Eds.), Atlas of Submarine Glacial Landforms: Modern, Quaternary and Ancient. Geological Society, London, Memoirs. vol. 46, pp. 71–72.

Camerlenghi, A., Domack, E., Rebesco, M., Gilbert, R., Ishman, S., Laventer, A., Brachfeld, S., Drake, A., 2002. Glacial morphology and post-glacial contourites in northern Prince Gustav Channel (NW Weddell Sea, Antarctica). Mar. Geophys. Res. 22, 417–443.

Campo, J.M., Wellner, J.S., Domack, E., Lavoie, C., Yoo, K.-C., 2017. Glacial geomorphology of the northwestern Weddell Sea, eastern Antarctic Peninsula continental shelf: shifting ice flow patterns during deglaciation. Geomorphology 280, 89–107.

Christie, F.D.W., Bingham, R.G., Gourmelen, N., Tett, S.F.B., Muto, A., 2016. Four-decade record of pervasive grounding line retreat along the Bellingshausen margin of West Antarctica. Geophys. Res. Lett. 43, 5741–5749.

Christie, F.D.W., Bingham, R.G., Gourmelen, N., Steig, E.J., Bisset, R.R., Pritchard, H.D., Snow, K., Tett, S.F.B., 2018. Glacier change along West Antarctica's Marie Byrd Land Sector and links to inter-decadal atmosphere-ocean variability. Cryosphere 12, 2461–2479.

Clark, C.D., Tulaczyk, S.M., Stokes, C.R., Canals, M.C., 2003. A groove-ploughing theory for the production of mega-scale glacial lineations, and implications for ice-stream mechanics. J. Glaciol. 149, 240–256.

Ó Cofaigh, C., Dowdeswell, J.A., 2001. Laminated sediments in glacimarine environments: diagnostic criteria for their interpretation. Quat. Sci. Rev. 20, 1411–1436.

Ó Cofaigh, C., Pudsey, C.J., Dowdeswell, J.A., Morris, P., 2002. Evolution of subglacial bedforms along a palaeo-ice stream, Antarctic Peninsula continental shelf. Geophysical Research Letters 29. https://doi.org/10.1029/2001GL014488.

Ó Cofaigh, C., Dowdeswell, J.A., Allen, C.S., Hiemstra, J., Pudsey, C.J., Evans, J., Evans, D.J.A., 2005. Flow dynamics and till genesis associated with a marine-based Antarctic palaeo-ice stream. Quat. Sci. Rev. 24, 709–740.

Ó Cofaigh, C., Evans, J., Dowdeswell, J.A., Larter, R.D., 2007. Till characteristics, genesis and transport beneath Antarctic paleo-ice streams. Journal of Geophysical Research: Earth Surface 112. https://doi.org/10.1029/2006JF000606.

Ó Cofaigh, C., et al., 2014. Reconstruction of ice-sheet changes in the Antarctic Peninsula since the last glacial maximum. Quat. Sci. Rev. 100, 87–110.

Cook, A.J., Vaughan, D.G., 2010. Overview of areal changes of the ice shelves on the Antarctic Peninsula over the past 50 years. Cryosphere 4, 77–98.

De Angelis, H., Skvarca, P., 2003. Glacier surge after ice shelf collapse. Science 299, 1560–1562.

Deacon, G.E.R., 1979. The Weddell gyre. Deep Sea Research Part A. Oceanographic Research Papers 26, 981–995.

Depoorter, M.A., Bamber, J.L., Griggs, J., Lenaerts, J.T.M., Ligtenberg, S.R.M., van den Broeke, M.R., Moholdt, G., 2013. Synthesized grounding line and ice shelf mask for Antarctica. PANGAEA https://doi.org/10.1594/PANGAEA.819151.

Doake, C.S.M., Vaughan, D.G., 1991. Rapid disintegration of the Wordie Ice Shelf in response to atmospheric warming. Nature 350, 328–330.

Domack, E., Leventer, A., Gilbert, R., Brachfeld, S., Ishman, S., Camerlenghi, A., Gavahan, K., Carlson, D., Barkoukis, A., 2001. Cruise reveals history of Holocene Larsen Ice Shelf. EOS Transactions, American Geophysical Union 82, 16–17.

Domack, E., Duran, D., Leventer, A., Ishman, S., Doane, S., McCallum, S., Amblas, D., Ring, J., Gilbert, R., Prentice, M., 2005. Stability of the Larsen B ice shelf on the Antarctic Peninsula during the Holocene epoch. Nature 436, 681–685.

Dowdeswell, J.A., et al., 2008b. Autonomous underwater vehicles (AUVs) and investigations of the ice-ocean interface in Antarctic and Arctic waters. J. Glaciol. 54, 661–672.

Dowdeswell, J.A., Bamber, J.L., 2007. Keel depths of modern Antarctic icebergs and implications for sea-floor scouring in the geological record. Mar. Geol. 243, 120–131.

Dowdeswell, J.A., Fugelli, E.M.G., 2012. The seismic architecture and geometry of grounding-zone wedges formed at the marine margins of past ice sheets. Bull. Geol. Soc. Am. 124, 1750–1761.

Dowdeswell, J.A., Hogan, K.A., 2016. Huge iceberg ploughmarks and associated corrugation ridges on the northern Svalbard shelf. In: Dowdeswell, J.A., Canals, M., Jakobsson, M., Todd, B.J., Dowdeswell, E.K., Hogan, K.A. (Eds.), Atlas of Submarine Glacial Landforms: Modern, Quaternary and Ancient. vol. 46. Geological Society, London, Memoirs, pp. 269–270.

Dowdeswell, J.A., Ottesen, D., 2016. Submarine landform-assemblage for Svalbard surge-type tidewater glaciers. In: Dowdeswell, J.A., Canals, M., Jakobsson, M., Todd, B.J., Dowdeswell, E.K., Hogan, K.A. (Eds.), Atlas of Submarine Glacial Landforms: Modern, Quaternary and Ancient. Geological Society, London, Memoirs. vol. 46, pp. 151–154.

Dowdeswell, J.A., Ottesen, D., Evans, J., Ó Cofaigh, C., Anderson, J.B., 2008a. Submarine glacial landforms and rates of ice-stream collapse. Geology 36, 819–822.

Dowdeswell, J.A., Villinger, H., Whittington, R.J., Marienfeld, P., 1993. Iceberg scouring in Scoresby Sund and on the East Greenland continental shelf. Mar. Geol. 111, 37–53.

Dowdeswell, J.A., Ó Cofaigh, C., Pudsey, C.J., 2004. Thickness and extent of the subglacial till layer beneath an Antarctic palaeo-ice stream. Geology 32, 13–16.

Dowdeswell, J.A., Hogan, K.A., Ó Cofaigh, C., Fugelli, E.M.G., Evans, J., Noormets, R., 2014. Late Quaternary ice flow in a West Greenland fjord and cross-shelf trough system: submarine landforms from Rink Isbrae to Uummannaq shelf and slope. Quat. Sci. Rev. 92, 292–309.

Dowdeswell, J.A., Batchelor, C.L., Montelli, A., Ottesen, D., Christie, F.D.W., Dowdeswell, E. K., Evans, J., 2020a. Delicate seafloor landforms reveal rapid Antarctic grounding-line retreat of kilometres per year. Science 368, 1020–1024.

Dowdeswell, J.A., Canals, M., Jakobsson, M., Todd, B.J., Dowdeswell, E.K., Hogan, K.A., 2016. The variety and distribution of submarine glacial landforms and implications for ice sheet reconstruction. In: Dowdeswell, J.A., Canals, M., Jakobsson, M., Todd, B.J., Dowdeswell, E.K., Hogan, K.A. (Eds.), Atlas of Submarine Glacial Landforms: Modern, Quaternary and Ancient. Geological Society, London, Memoirs. vol. 46, pp. 519–552.

Dowdeswell, J.A., Batchelor, C.L., Dorschel, B., Benham, T.J., Christie, F.D.W., Dowdeswell, E. K., Montelli, A., Arndt, J.E., Gebhardt, C., 2020b. Sea-floor and sea-ice conditions in the western Weddell Sea, Antarctica, around the wreck of Sir Ernest Shackleton's *Endurance*. Antarct. Sci. 32, 301–313.

Evans, J., Hogan, K.A., 2016. Grounding-zone wedges on the northern Larsen shelf, Antarctic Peninsula. In: Dowdeswell, J.A., Canals, M., Jakobsson, M., Todd, B.J., Dowdeswell, E.K., Hogan, K.A. (Eds.), Atlas of Submarine Glacial Landforms: Modern, Quaternary and Ancient. Geological Society, London, Memoirs. vol. 46, pp. 237–238.

Evans, J., Pudsey, C.J., 2002. Sedimentation associated with Antarctic Peninsula ice shelves: implications for palaeoenvironmental reconstructions of glacimarine sediments. J. Geol. Soc. Lond. 159, 233–238.

Evans, D.J.A., Rea, B.R., 1999. Geomorphology and sedimentology of surging glaciers: a land-systems approach. Ann. Glaciol. 28, 75–82.

Evans, J., Pudsey, C.J., Ó Cofaigh, C., Morris, P.W., Domack, E.W., 2005. Late Quaternary glacial history, dynamics and sedimentation of the eastern margin of the Antarctic Peninsula Ice Sheet. Quat. Sci. Rev. 24, 741–774.

Evans, J., Dowdeswell, J.A., Ó Cofaigh, C., Benham, T.J., Anderson, J.B., 2006. Extent and dynamics of the West Antarctic Ice Sheet on the outer continental shelf of Pine Island Bay during the last glaciation. Mar. Geol. 230, 53–72.

Fahnestock, M.A., Abdalati, W., Shuman, C., 2002. Long melt seasons on ice shelves of the Antarctic Peninsula: an analysis using satellite-based microwave emission measurements. Ann. Glaciol. 34, 127–133.

Fowler, A.C., Chapwanya, M., 2014. An instability theory for the formation of ribbed moraine, drumlins and mega-scale glacial lineations. Proceedings of the Royal Society A 470, 20140185.

Gilbert, R., Domack, E.W., Camerlenghi, A., 2003. Deglacial history of the Greenpeace Trough: ice sheet to ice shelf transition in the northern Weddell Sea. In: Domack, E., Leventer, A., Burnett, A., Bindschadler, R., Convey, P., Kirby, M. (Eds.), Antarctic Peninsula Climate Variability: Historical and Palaeoenvironmental Perspectives. Antarctic Research Series vol. 79. AGU, Washington, DC, pp. 195–204.

Graham, A.G.C., Dutrieux, P., Vaughan, D.G., Nitsche, F.O., Gyllencreutz, R., Greenwood, S.L., Larter, R.D., Jenkins, A., 2013. Seabed corrugations beneath an Antarctic ice shelf revealed by autonomous underwater vehicle survey: origin and implications for the history of Pine Island Glacier. Journal of Geophysical Research: Earth Surface 118, 1356–1366.

Greenwood, S.J., Gyllencreutz, R., Jakobsson, M., Anderson, J.B., 2012. Ice-flow switching and East/West Antarctic Ice Sheet roles in glaciation of the western Ross Sea. Geol. Soc. Am. Bull. 124, 1736–1749.

Gwyther, D.E., Galton-Fenzi, B.K., Dinniman, M.S., Roberts, J.L., Hunter, J.R., 2015. The effect of basal friction on melting and freezing in ice shelf-ocean models. Ocean Model. 95, 38–52.

Halberstadt, A.R.W., Simkins, L.M., Greenwood, S.L., Anderson, J.B., 2016. Past ice-sheet behaviour: retreat scenarios and changing controls in the Ross Sea, Antarctica. Cryosphere 10, 1003–1020.

Heroy, D.C., Anderson, J.B., 2005. Ice-sheet extent of the Antarctic Peninsula region during the Last Glacial Maximum (LGM) — insights from glacial geomorphology. Geol. Soc. Am. Bull. 117, 1497–1512.

Howat, I.M., Porter, C., Smith, B.E., Noh, M.-J., Morin, P., 2019. The reference elevation model of Antarctica. Cryosphere 13, 665–674.

Howe, J.A., Husum, K., Inall, M.E., Coogan, J., Luckman, A., Arosio, R., Abernethy, C., Verchili, D., 2019. Autonomous underwater vehicle (AUV) observations of recent tidewater glacier retreat, western Svalbard. Mar. Geol. 417, 106009.

Jakobsson, M., Anderson, J.B., 2016. Corrugation ridges in the Pine Island Bay glacier trough, West Antarctica. In: Dowdeswell, J.A., Canals, M., Jakobsson, M., Todd, B.J., Dowdeswell, E.K., Hogan, K.A. (Eds.), Atlas of Submarine Glacial Landforms: Modern, Quaternary and Ancient. Geological Society, London, Memoirs. vol. 46, pp. 265–266.

Jakobsson, M., et al., 2011. Geological record of ice shelf break-up and grounding line retreat, Pine Island Bay, West Antarctica. Geology 39, 691–694.

Jakobsson, M., Gyllencreutz, R., Mayer, L.A., Dowdeswell, J.A., Canals, M., Todd, B.J., Dowdeswell, E.K., Hogan, K.A., Larter, R.D., 2016. Mapping submarine glacial landforms using acoustic methods. In: Dowdeswell, J.A., Canals, M., Jakobsson, M., Todd, B.J., Dowdeswell, E.K., Hogan, K.A. (Eds.), Atlas of Submarine Glacial Landforms: Modern, Quaternary and Ancient. Geological Society, London, Memoirs. vol. 46, pp. 17–40.

Khazendar, A., et al., 2016. Rapid submarine ice melting in the grounding zones of ice shelves in West Antarctica. Nat. Commun. 7, 13243.

Kim, K., Jezek, K.C., Liu, H., 2007. Orthorectified image mosaic of Antarctica from 1963 Argon satellite photography: image processing and glaciological applications. Int. J. Remote Sens. 28, 5357–5373.

King, J.C., 1994. Recent climate variability in the vicinity of the Antarctic Peninsula. Int. J. Climatol. 14, 357–369.

King, L.H., Rokoengen, K., Fader, G.B.J., Gunleiksrud, T., 1991. Till-tongue stratigraphy. Geol. Soc. Am. Bull. 103, 637–659.

King, E.C., Hindmarsh, R.C.A., Stokes, C.R., 2009. Formation of mega-scale glacial lineations observed beneath a West Antarctic ice stream. Nat. Geosci. 2, 585–588.

Klages, J.P., Kuhn, G., Graham, A.G.C., Hillenbrand, C.-D., Smith, J.A., Nitsche, F.O., Larter, R.D., 2015. Palaeo-ice stream pathways and retreat style in the easternmost Amundsen Sea Embayment, West Antarctica, revealed by combined multibeam bathymetric and seismic data. Geomorphology 245, 207–222.

Kurtz, N.T., Markus, T., 2012. Satellite observations of Antarctic Sea ice thickness and volume. J. Geophys. Res. 117, C08025.

Larter, R.D., Vanneste, L.E., 1995. Relict subglacial deltas on the Antarctic Peninsula outer shelf. Geology 23, 33–36.

Larter, R.D., et al., 2019. Subglacial hydrological control on flow of an Antarctic Peninsula palaeo-ice stream. Cryosphere 13, 1583–1596.

Lavoie, C., et al., 2015. Configuration of the Northern Antarctic Peninsula Ice Sheet at LGM based on a new synthesis of seabed imagery. Cryosphere 9, 613–629.

Licht, K.J., Dunbar, N.W., Andrews, J.T., Jennings, A.E., 1999. Distinguishing subglacial till and glacial marine diamictons in the western Ross Sea, Antarctica: implications for a last glacial maximum grounding line. Geol. Soc. Am. Bull. 111, 91–103.

Lien, R., Solheim, A., Elverhøi, A., Rokoengen, K., 1989. Iceberg scouring and sea bed morphology on the eastern Weddell Sea shelf, Antarctica. Polar Res. 7, 43–57.

Linch, L., van der Meer, J.J.M., Menzies, J., 2012. Micromorphology of iceberg scour in clays: glacial Lake Agassiz, Manitoba, Canada. Quat. Sci. Rev. 55, 125–144.

Livingstone, S.J., Ó Cofaigh, C., Hogan, K.A., Dowdeswell, J.A., 2016. Submarine glacial-landform distribution along an Antarctic Peninsula palaeo-ice stream: a shelf – slope transect through the Marguerite Trough system (66–70° S). In: Dowdeswell, J.A., Canals, M., Jakobsson, M., Todd, B.J., Dowdeswell, E.K., Hogan, K.A. (Eds.), Atlas of Submarine Glacial Landforms: Modern, Quaternary and Ancient. Geological Society, London, Memoirs. vol. 46, pp. 485–492.

Lowe, A.L., Anderson, J.B., 2003. Evidence for abundant subglacial meltwater beneath the paleo-ice sheet in Pine Island Bay, Antarctica. J. Glaciol. 49, 125–138.

Lurton, X., 2010. An Introduction to Underwater Acoustics: Principles and Applications. Springer Praxis Publishing. Mareano website http://www.mareano.no/en.

Metz, J.M., Dowdeswell, J.A., Woodworth-Lynas, C.M.T., 2008. Sea-floor scour at the mouth of Hudson Strait by deep-keeled icebergs from the Laurentide ice sheet. Mar. Geol. 253, 149–159.

Montelli, A., Dowdeswell, J.A., Ottesen, D., Johansen, S.E., 2017. Ice-sheet dynamics through the Quaternary on the mid-Norwegian continental margin inferred from 3D seismic data. Mar. Pet. Geol. 80, 228–242.

Montelli, A., Dowdeswell, J.A., Ottesen, D., Johansen, S.E., 2018. 3D seismic evidence of buried iceberg ploughmarks from the mid-Norwegian continental margin reveals largely persistent North Atlantic Current through the Quaternary. Mar. Geol. 399, 66–83.

Morris, E.M., Vaughan, D.G., 2003. Spatial and temporal variation of surface temperature on the Antarctic Peninsula and the limit of variability of ice shelves. Antarctic Research Series 79, 61–68.

Muench, R.D., Gordon, A.L., 1995. Circulation and transport of water along the western Weddell Sea margin. J. Geophys. Res. 100, 18503–18515.

Newton, A.M.W., Huuse, M., Brocklehurst, S.H., 2016. Buried iceberg scours reveal reduced North Atlantic Current during the stage 12 deglacial. Nat. Commun. 7, 10927.

O'Brien, P.E., De Santis, L., Harris, P.T., Domack, E., Quilty, P.G., 1999. Ice shelf grounding zone features of western Prydz Bay, Antarctica: sedimentary processes from seismic and sidescan images. Antarct. Sci. 11, 78–91.

Ødegård, Ø., Hansen, R.E., Singh, H., Maarleveld, T.J., 2018. Archaeological use of Synthetic Aperture Sonar on deepwater wreck sites in Skagerrak. Journal of Archaeological Science 89, 1–13 Ocean Mapping Group website:. www.omg.unb.ca/Projects/Arctic/.

OMG Mission, 2016. Bathymetry (sea floor depth) data from the ship-based bathymetry survey. OMG SDS, CA, USA. https://doi.org/10.5067/OMGEV-BTYSS.

Ottesen, D., Dowdeswell, J.A., 2006. Assemblages of submarine landforms produced by tidewater glaciers in Svalbard. Journal of Geophysical Research 111. https://doi.org/10.1029/2005JF000330.

Ottesen, D., Dowdeswell, J.A., Rise, L., 2005. Submarine landforms and the reconstruction of fast-flowing ice streams within a large Quaternary ice sheet: the 2500-km-long Norwegian-Svalbard margin (57° to 80°N). Geol. Soc. Am. Bull. 117, 1033–1050.

Ottesen, D., Dowdeswell, J.A., Lanvik, J.Y., Mienert, J., 2007. Dynamics of the Late Weichselian ice sheet on Svalbard inferred from high-resolution sea-floor morphology. Boreas 36, 286–306.

Ottesen, D., Stokes, C.R., Rise, L., Olsen, L., 2008. Ice-sheet dynamics and ice streaming along the coastal parts of northern Norway. Quat. Sci. Rev. 27, 922–940.

Powell, R.D., Alley, R.B., 1997. Grounding-line systems: processes, glaciological inferences and the stratigraphic record. In: Barker, P.F., Cooper, A.C. (Eds.), Geology and Seismic Stratigraphy of the Antarctic Margin II. Antarctic Research Series vol. 71, pp. 169–187.

Pritchard, H.D., Arthern, R.J., Vaughan, D.G., Edwards, L.A., 2009. Extensive dynamic thinning on the margins of the Greenland and Antarctic ice sheets. Nature 461, 971–975.

Pudsey, C.J., Evans, J., 2001. First survey of Antarctic sub-ice shelf sediments reveals Mid-Holocene ice shelf retreat. Geology 29, 787–790.

Pudsey, C.J., Evans, J., Domack, E.W., Morris, P., Del Valle, R., 2001. Bathymetry and acoustic facies beneath the former Larsen-A and Prince Gustav Ice Shelves, NW Weddell Sea. Antarct. Sci. 13, 312–322.

Pudsey, C.J., Murray, J.W., Appleby, P., Evans, J., 2006. Ice shelf history from petrographic and foraminiferal evidence, Northeast Antarctic Peninsula. Quat. Sci. Rev. 25, 2357–2379.

Rack, W., Rott, H., 2004. Pattern of retreat and disintegration of Larsen B Ice Shelf, Antarctic Peninsula. Ann. Glaciol. 39, 505–510.

Reinardy, B.T.I., Hiemstra, J.F., Murray, T., Hillenbrand, C.-D., Larter, R.D., 2011. Till genesis at the bed of an Antarctic Peninsula palaeo-ice stream as indicated by micromorphological analysis. Boreas 40, 498–517.

Rignot, E., Casassa, G., Gogineni, P., Krabill, W., Rivera, A., Thomas, R., 2004. Accelerated ice discharge from the Antarctic Peninsula following the collapse of Larsen B ice shelf. Geophysical Research Letters, 31 https://doi.org/10.1029/2004GL020697.

Rignot, E., Mouginot, J., Morlighem, M., Seroussi, H., Scheuchl, B., 2014. Widespread, rapid grounding line retreat of Pine Island, Thwaites, Smith, and Kohler glaciers, West Antarctica, from 1992 to 2011. Geophys. Res. Lett. 41, 3502–3509.

Rignot, E., Mouginot, J., Scheuchl, B., van den Broeke, M., van Wessem, M.J., Morlighem, M., 2019. Four decades of Antarctic Ice Sheet mass balance from 1979–2017. Proceedings of the National Academy of Sciences of the United States of America 116, 1095–1103.

Rott, H., Skvarca, P., Nagler, T., 1996. Rapid collapse of the Northern Larsen Ice Shelf, Antarctica. Science 271, 788–792.

Rott, H., Rack, W., Skvarca, P., De Angelis, H., 2002. Northern Larsen Ice Shelf, Antarctica: further retreat after collapse. Ann. Glaciol. 34, 277–282.

Rott, H., Müller, F., Nagler, T., Floricioiu, D., 2011. The imbalance of glaciers after disintegration of Larsen-B ice shelf, Antarctic Peninsula. Cryosphere 5, 125–134.

Rott, H., Abdel Jaber, W., Wuite, J., Scheiblauer, S., Floricioiu, D., Van Wessem, J.M., Nagler, T., Miranda, N., Van Den Broeke, M.R., 2018. Cryosphere 12, 1273–1291.

Rydningen, T.A., Vorren, T.O., Laberg, J.S., Kolstad, V., 2013. The marine-based NW Fennoscandian ice sheet: glacial and deglacial dynamics as reconstructed from submarine landforms. Quat. Sci. Rev. 68, 126–141.

Scambos, T., Hulbe, C., Fahnestock, M., 2003. Climate-induced ice shelf disintegration in the Antarctic Peninsula. In: Domack, E., Leventer, A., Burnett, A., Bindschadler, R., Convey, P., Kirby, M. (Eds.), Antarctic Peninsula Climate Variability: Historical and Palaeoenvironmental Perspectives. vol. 79. Antarctic Research Series, AGU, Washington, DC, pp. 79–92.

Sæbø, T.O., Synnes, S.A.V., Hansen, R.E., 2013. Wideband interferometry in synthetic aperture sonar. IEEE Trans. Geosci. Remote Sens. 51, 4450–4459.

Scambos, T.A., Bohlander, J.A., Shuman, C.A., Skvarca, P., 2004. Glacier acceleration and thinning after ice shelf collapse in the Larsen B embayment, Antarctica. Geophysical Research Letters 31. https://doi.org/10.1029/2004/GL020670.

Scheuchl, B., Mouginot, J., Rignot, E., Morlighem, M., Khazendar, A., 2016. Grounding line retreat of Pope, Smith, and Kohler Glaciers, West Antarctica, measured with Sentinel-1a radar interferometry data. Geophys. Res. Lett. 43, 8572–8579.

Schodlok, M.P., Hellmer, H.H., Rohardt, G., Fahrbach, E., 2006. Weddell Sea iceberg drift: five years of observations. Journal of Geophysical Research: Oceans 111. https://doi.org/10.1029/2004JC002661.

Shaw, J., Pugin, A., Young, R.R., 2008. A meltwater origin for Antarctic shelf bedforms with special attention to megalineations. Geomorphology 102, 364–375.

Shepherd, A., Wingham, D., Rignot, E., 2004. Warm ocean is eroding West Antarctic Ice Sheet. Geophys. Res. Lett. 31, L23402.

Shepherd, A., et al., 2018. Mass balance of the Antarctic Ice Sheet from 1992 to 2017. Nature 558, 219–222.

Simkins, L.M., Anderson, J.B., Greenwood, S.L., Gonnermann, H.M., Prothro, L.O., Halberstadt, A.R.W., Stearns, L.A., Pollard, D., DeConto, R.M., 2017. Anatomy of a meltwater drainage system beneath the ancestral East Antarctic ice sheet. Nat. Geosci. 10, 691–697.

Simkins, L.M., Greenwood, S.L., Anderson, J.B., 2018. Diagnosing ice sheet grounding line stability from landform morphology. Cryosphere 12, 2707–2726.

Skvarca, P., Rack, W., Rott, H., Ibarzabal y Donangelo, T., 1999. Climatic trend and the retreat and disintegration of ice shelves on the Antarctic Peninsula: an overview. Polar Res. 18, 151–157.

Sloan, B.J., Lauver, L.A., Anderson, J.B., 1995. Seismic stratigraphy of the Larsen Basin, eastern Antarctic Peninsula. Antarctic Research Series 68, 59–74.

Smedley, R.K., et al., 2017. Internal dynamics condition centennial-scale oscillations in marine-based ice-stream retreat. Geology 45, 787–790.

Smith, J.A., Graham, A.G.C., Post, A.L., Hillenbrand, C.-D., Bart, P.J., Powell, R.D., 2019. The marine geological imprint of Antarctic ice shelves. Nat. Commun. 10, 5635.

Spagnolo, M., Clark, C.D., Ely, J.C., Stokes, C.R., Anderson, J.B., Andreassen, K., Graham, A.G. C., King, E.C., 2014. Size, shape and spatial arrangement of mega-scale glacial lineations from a large and diverse dataset. Earth Surf. Process. Landf. 39, 1432–1448.

Spagnolo, M., Phillips, E., Piotrowski, J.A., Rea, B.R., Clark, C.D., Stokes, C.R., Carr, S.J., Ely, J. C., Ribolini, A., Wysota, W., Szuman, I., 2016. Ice stream motion facilitated by a shallow-deforming and accreting bed. Nat. Commun. 7, 10723.

Stoker, M.S., 1988. Pleistocene ice-proximal glaciomarine sediments in boreholes from the Hebrides Shelf and Wyville-Thomson Ridge, NW UK continental shelf. Scott. J. Geol. 24, 249–262.

Stokes, C.R., Clark, C.D., 1999. Geomorphological criteria for identifying Pleistocene ice streams. Ann. Glaciol. 28, 67–74.

Stokes, C.R., Clark, C.D., 2002. Are long subglacial bedforms indicative of fast ice flow? Boreas 31, 239–249.

Stokes, C.R., Spagnolo, M., Clark, C.D., 2011. The composition and internal structure of drumlins: complexity, commonality, and implications for a unifying theory of their formation. Earth-Surface Reviews 107, 398–422.

Stokes, C.R., Spagnolo, M., Clark, C.D., Ó Cofaigh, C., Lian, O.B., Dunstone, R.B., 2013. Formation of mega-scale glacial lineations on the Dubawnt Lake Ice Stream bed: 1. Size, shape and spacing from a large remote sensing dataset. Quat. Sci. Rev. 77, 190–209.

Taylor, J., Siegert, M.J., Payne, A.J., Hubbard, B., 2004. Regional-scale bed roughness beneath ice masses: measurement and analysis. Comput. Geosci. 30, 899–908.

The RAISED Consortium, 2014. A community-based geological reconstruction of Antarctic Ice Sheet deglaciation since the Last Glacial Maximum. Quat. Sci. Rev. 100, 1–9.

Todd, B.J., Lewis, C.F.M., Ryall, P.J.C., 1988. Comparison of trends of iceberg scour marks with iceberg trajectories and evidence of paleocurrent trends on Saglek Bank, northern Labrador Shelf. Can. J. Earth Sci. 25, 1374–1383.

Vaughan, D.G., Doake, C.S.M., 1996. Recent atmospheric warming and retreat of ice shelves on the Antarctic Peninsula. Nature 379, 328–331.

Vaughan, D.G., Marshall, G.J., Connolley, W.M., Parkinson, C., Mulvaney, R., Hodgson, D.A., King, J.C., Pudsey, C.J., Turner, J., 2003. Recent rapid regional climate warming on the Antarctic Peninsula. Clim. Chang. 60, 243–274.

Wise, M.G., Dowdeswell, J.A., Jakobsson, M., Larter, R.D., 2017. Evidence of marine ice-cliff instability in Pine Island Bay from iceberg-keel plough marks. Nature 550, 506–510.

Woodworth-Lynas, C.M.T., Josenhans, H.W., Barrie, J.V., Lewis, C.F.M., Parrott, D.R., 1991. The physical processes of seabed disturbance during iceberg grounding and scouring. Cont. Shelf Res. 11, 939–961.